

MICROCOPY RESOLUTION TEST CHART  
NATIONAL BUREAU OF STANDARDS 1963-A

AD-A176 939

12

AFGL-TR-86-0261

PROGRESS TOWARD PREDICTING HIGH-VOLTAGE CHARGING OF SPACECRAFT IN LOW POLAR ORBIT

J.G. Laframboise  
L.W. Parker

Physics Department  
York University  
4700 Keele Street  
Downsview, Ontario M3J 1P3  
Canada

DTIC  
ELECTE  
FEB 20 1987  
S D

28 October 1986

Scientific Report No. 2

APPROVED FOR PUBLIC RELEASE: DISTRIBUTION UNLIMITED

AIR FORCE GEOPHYSICS LABORATORY  
AIR FORCE SYSTEMS COMMAND  
UNITED STATES AIR FORCE  
HANSCOM AIR FORCE BASE, MASSACHUSETTS 01731

DTIC FILE COPY

87 2 19 198

"This technical report has been reviewed and is approved for publication"

*Allen Rubin*

ALLEN RUBIN  
Contract Manager  
Spacecraft Interactions Branch  
Space Physics Division

*Charles P. Pike*

CHARLES P. PIKE, Chief  
Spacecraft Interactions Branch  
Space Physics Division

FOR THE COMMANDER

*John A. Gaudet*

JOHN A. GAUDET, Major, USAF/Acting Director  
Space Physics Division

This report has been reviewed by the ESD Public Affairs Office (PA) and is releasable to the National Technical Information Service (NTIS).

Qualified requestors may obtain additional copies from the Defense Technical Information Center. All others should apply to the National Technical Information Service.

If your address has changed, or if you wish to be removed from the mailing list, or if the addressee is no longer employed by your organization, please notify AFGL/DAA, Hanscom AFB, MA 01731. This will assist us in maintaining a current mailing list.

Do not return copies of this report unless contractual obligations or notices on a specific document requires that it be returned.

REPORT DOCUMENTATION PAGE

1a. REPORT SECURITY CLASSIFICATION unclassified			1b. RESTRICTIVE MARKINGS		
2a. SECURITY CLASSIFICATION AUTHORITY			3. DISTRIBUTION/AVAILABILITY OF REPORT Approved for public release; Distribution unlimited.		
2b. DECLASSIFICATION/DOWNGRADING SCHEDULE			4. PERFORMING ORGANIZATION REPORT NUMBER(S)		
4. PERFORMING ORGANIZATION REPORT NUMBER(S)			5. MONITORING ORGANIZATION REPORT NUMBER(S) AFGL-TR-86-0261		
6a. NAME OF PERFORMING ORGANIZATION York University		6b. OFFICE SYMBOL (If applicable)	7a. NAME OF MONITORING ORGANIZATION Air Force Geophysics Laboratory		
6c. ADDRESS (City, State and ZIP Code) 4700 Keele Street Downsview, Ontario, Canada M3J 1P3			7b. ADDRESS (City, State and ZIP Code) Hanscom AFB Massachusetts 01731		
8a. NAME OF FUNDING/SPONSORING ORGANIZATION Air Force Geophysics Laboratory		8b. OFFICE SYMBOL (If applicable)	9. PROCUREMENT INSTRUMENT IDENTIFICATION NUMBER F19628-S3-K-0023		
8c. ADDRESS (City, State and ZIP Code) Hanscom AFB Massachusetts 01731			10. SOURCE OF FUNDING NOS		
			PROGRAM ELEMENT NO 62101F	PROJECT NO 7661	TASK NO 11
			WORK UNIT NO AC		
11. TITLE (Include Security Classification) Progress toward Predicting High-Voltage Charging of Spacecraft in Low Polar Orbit					
12. PERSONAL AUTHOR(S) J.G. Laframboise, L. W. Parker*					
13a. TYPE OF REPORT Scientific Report #2		13b. TIME COVERED FROM 15/07/84 to 14/07/85	14. DATE OF REPORT (Yr., Mo., Day) 1986 October 23		15. PAGE COUNT 66
16. SUPPLEMENTARY NOTATION * Lee W. Parker, Inc, 252 Lexington Road, Concord, MA 01742					
17. COSATI CODES			18. SUBJECT TERMS (Continue on reverse if necessary and identify by block number)		
FIELD	GROUP	SUB. GR	Spacecraft charging Low Polar Orbit		
			Auroral Ionosphere Electron Escape		
19. ABSTRACT (Continue on reverse if necessary and identify by block number) This annual report consists of two submitted papers, one to a Conference and one to a Journal. Section 2 of this report is a paper presented at the NATO AGARD Spring 1986 Electro-magnetic Wave Propagation Panel Symposium on "The Aerospace Environment at High Altitudes and its Implications for Spacecraft Charging and Communications", The Hague, Netherlands, 2-6 June 1986. This paper is primarily of a "survey" nature, and contains relatively brief accounts of several aspects of the low polar-orbit high-voltage charging problem. However, its Section 3 presents the first results from L.W. Parker's simulation work which was supported by this Contract. Section 3 of this report contains the text of a paper submitted in October 1986 for publication in Journal of Geophysical Research, Space Physics. It is an expanded version of an earlier paper by Laframboise (1985) on secondary electron escape from negatively charged spacecraft surfaces in a magnetic field, and now includes results for situations in which there exist electric fields tangential as well as normal to the surface.					
20. DISTRIBUTION/AVAILABILITY OF ABSTRACT UNCLASSIFIED/UNLIMITED <input checked="" type="checkbox"/> SAME AS RPT <input type="checkbox"/> DTIC USERS <input type="checkbox"/>			21. ABSTRACT SECURITY CLASSIFICATION Unclassified		
22a. NAME OF RESPONSIBLE INDIVIDUAL A.G. Rubin			22b. TELEPHONE NUMBER (Include Area Code) 617-377-2933	22c. OFFICE SYMBOL AFGL/PHK	

**TABLE OF CONTENTS**

1.	Introduction	1
2.	Paper: "Spacecraft Charging in the Auroral Plasma: Progress toward Understanding the Physical Effects Involved"	3
	Abstract	3
	2.1 Introduction	3
	2.2 Calculation of Secondary-Electron Escape Currents from Negatively-Charged Surfaces in a Magnetic Field	4
	2.3 Estimate of Required Environmental Conditions for Low-Polar-Orbit Charging	5
	2.4 Results from a Numerical Simulation	9
	References	11
	Table	13
	Figures	13
3.	Paper: "Calculation of Secondary-Electron Escape Currents from Negatively-Charged Surfaces in a Magnetic Field"	18
	Abstract	19
	3.1 Introduction	20
	3.2 Theory for E Normal to Surface	23
	3.3 Results and Discussion for E Normal to Surface	29
	3.4 Theory for Non-Normal Directions of E	31
	3.5 Results and Discussion for Non-Normal Directions of E	34
	3.6 Calculation of Secondary-Electron Densities	38
	References	39
	Table	41
	Figures	42

Distribution For	
CRA&I	<input checked="" type="checkbox"/>
TAB	<input type="checkbox"/>
Unprocessed	<input type="checkbox"/>
Location	

Availability Codes

Dist	Avail and/or Special
A-1	



## 1. INTRODUCTION

This annual report covers the second year of Contract No. F19628-83-K-0028. It consists of two submitted papers, one to a Conference and one to a Journal.

Section 2 of this report is a paper presented at the NATO AGARD Spring 1986 Electromagnetic Wave Propagation Panel Symposium on "The Aerospace Environment at High Altitudes and its Implications for Spacecraft Charging and Communications", The Hague, Netherlands, 2-6 June 1986. This paper is primarily of a "survey" nature, and contains relatively brief accounts of several aspects of the low-polar-orbit high-voltage charging problem. However, its Section 4 presents the first results from L.W. Parker's simulation work which was supported by this Contract. We believe that his study is the first calculation of downstream potentials on electrically-isolated surfaces which is based on the use of ion orbit integrations for calculating current deposition on such surfaces. The successful completion of this work involved overcoming extreme numerical difficulties. These appear to be closely associated with physical sensitivities inherent in the physics of high-voltage ion wakes, particularly in regard to the extremely beam-like character of the ion velocity distributions in such wakes. This situation has severe implications for the ability to make economical, realistic predictions of high-voltage charging in geometrically-complicated situations, including arrangements of exposed equipment boxes in the Shuttle's cargo bay, and much of the Space Station's proposed Polar Platform.

Section 3 of this report contains the text of a paper submitted in October 1986 for publication in Journal of Geophysical Research, Space Physics. It is an expanded version of an earlier paper by Laframboise (1985) on secondary-electron escape from negatively-charged spacecraft surfaces in a magnetic field, and now includes results for situations in which there exist electric fields tangential as well as normal to such surfaces.

**SPACECRAFT CHARGING IN THE AURORAL PLASMA:  
PROGRESS TOWARD UNDERSTANDING THE PHYSICAL EFFECTS INVOLVED**

J.G. Laframboise\* and L.W. Parker\*\*

\*Physics Department, York University, Toronto, Canada M3J 1P3

\*\*Lee W. Parker, Inc., 252 Lexington Rd., Concord, Mass., U.S.A., 01742

**ABSTRACT**

The work presented here is in four parts. In the first, we review the main differences between the plasma environments in geostationary orbit and low polar orbit with regard to high-voltage charging situations. We next present results from a calculation of secondary-electron escape currents from negatively-charged spacecraft surfaces having various orientations relative to the local magnetic-field direction. We show that for finite ranges of combinations of electric and magnetic field directions, secondary-electron escape is completely suppressed and therefore cannot help to discharge the spacecraft. In such circumstances, secondary electrons may travel distances many times their gyroradii before reimpacting, and this may produce greatly increased secondary-electron surface currents. Thirdly, we develop a simple rough estimate of the required conditions for high-voltage auroral-zone charging. The results suggest that for any given spacecraft, surface potentials are likely to depend more strongly on the ratio of ambient flux of high-energy electrons to that of all ions, than on any other environmental parameter. Finally, we present preliminary results of numerical simulation work directed toward testing this hypothesis. Numerical instabilities encountered in doing this simulation work probably are closely related to physical sensitivities inherent in the physics of the ion wake behind the spacecraft, and especially to beam-like constituents of the ion population in the wake.

**1. INTRODUCTION**

The plasma environment in low Earth orbit has very different properties from that in geostationary orbit. In **GEOSTATIONARY ORBIT**:

- (a) the Debye Length is a few tens of metres; therefore, **SPACE-CHARGE COUPLING** is **SMALL**, and one can ignore it entirely, or use a linearized approximation for it, when calculating potentials near spacecraft of "ordinary" size.
- (b) average particle gyroradii are a few tens of metres or larger; therefore **MAGNETIC-FIELD EFFECTS ARE NEGLIGIBLE** for calculating particle orbits, near spacecraft of "ordinary" size.
- (c) circular-orbit speed is much smaller than particle average random speeds; therefore, **AMBIENT PARTICLE DISTRIBUTIONS CAN "USUALLY" BE ASSUMED ISOTROPIC**, and this greatly simplifies calculations of ambient-particle currents collected by spacecraft. In reality, significant anisotropies are observed in ambient particle distributions, but these are generally less important than the relative ion anisotropy induced in low orbit by spacecraft motion.

In **LOW EARTH ORBIT**, none of the above are true. Space-charge coupling is strong, magnetic-field effects are strong, and ion flow effects are important. Also, charged-particle mean free paths may not always be much larger than spacecraft size, especially during thruster firings and water dumps.

Table 1 summarizes some important characteristic lengths and speeds for low-orbit conditions. A surprising feature of this Table is that the sheath thicknesses indicated are much larger than the ambient Debye Length, but this is because the sheath potentials are much larger than the ambient-particle thermal energies. These distances are at most comparable to typical spacecraft dimensions, in contrast with the geosynchronous situation. Table 1 also shows that secondary electrons have an average gyroradius  $\ll$  typical spacecraft dimensions, so their escape will be inhibited strongly on surfaces which are nearly parallel to the magnetic field  $B$  (Fig. 1), while auroral electrons have an average gyroradius  $\geq$  typical spacecraft dimensions, so their collection will be affected only moderately, except for very large spacecraft. We return to this question in Sec. 2. Also evident from Table 1 is the large value of the ion speed ratio (spacecraft speed/ion most-probable thermal speed) in low-orbit conditions. In these conditions, ion collection on downstream surfaces will be inhibited. If a surface is simultaneously downstream and nearly parallel to the magnetic field, as is likely to be the case in the auroral zones, then the tendency for high-voltage charging to occur on it will be greatly increased (Fig. 2).

In the rest of this paper, we report briefly on three separate projects. In Sec. 2, we present results of a calculation of secondary-electron escape currents from negatively-charged surfaces having various orientations relative to the local magnetic-field direction. In Sec. 3, we develop a simple rough estimate of the required conditions for high-voltage charging. The results suggest that for any given spacecraft, surface potentials are likely to depend more strongly on the ratio of ambient flux of high-energy electrons to that of all ions, than on any other environmental parameter. In Sec. 4, we present results of numerical simulation work directed toward testing this hypothesis. This work involves calculations of floating-potential distributions on infinite cylinders in collisionless plasma crossflows whose properties model those of the auroral plasma.

## 2. CALCULATION OF SECONDARY-ELECTRON ESCAPE CURRENTS FROM NEGATIVELY-CHARGED SURFACES IN A MAGNETIC FIELD.

Figure 2 illustrates why escape of secondary electrons is affected by magnetic fields. In Fig. 2(a), the spacecraft surface is perpendicular to  $\mathbf{B}$ , and the emitted electrons, which experience an electric force  $-e\mathbf{E}$  directed away from the surface, all escape, helping to discharge it. Here  $e$  is the magnitude of the electronic charge. In Fig. 2(b), the spacecraft surface is nearly parallel to  $\mathbf{B}$ , and almost all of the emitted electrons return to it, even though they still experience an electric force directed away from it. These electrons therefore are unable to help discharge it, so a surface nearly parallel to  $\mathbf{B}$  is more likely to charge to a large negative voltage. The component of  $\mathbf{E}$  which is perpendicular to  $\mathbf{B}$  results only in an  $\mathbf{E} \times \mathbf{B}$  drift parallel to the surface.

In this Section, we present numerically-calculated escaping secondary-electron fluxes for these conditions, for the case when the electric field  $\mathbf{E}$  is normal to the surface. We also indicate some general properties of the escaping flux when  $\mathbf{E}$  has a nonzero tangential component, i.e., the surface is at a nonuniform potential.

We assume that the surface is flat, that  $\mathbf{E}$  and  $\mathbf{B}$  are uniform, and that secondary electrons are emitted with a Maxwellian velocity distribution corresponding to a temperature  $T$ . If  $-e\mathbf{E}$  is directed along the outward surface normal, then the ratio  $\epsilon = I/I_0$  of escaping to emitted flux is a function of only two parameters: the angle  $\theta$  between the surface normal and the direction of  $\mathbf{B}$  (Fig. 3), and a parameter describing the strength of  $\mathbf{E}$ . A convenient choice for this parameter is the difference in potential across a mean secondary-electron gyroradius  $\bar{a} = (1/eB) (\pi mkT/2)^{1/2}$ , divided by  $kT/e$ , where  $m$  is electron mass and  $k$  is Boltzmann's constant. This quotient is:

$$\epsilon = \frac{E}{B} \sqrt{\frac{\pi m}{2kT}} \quad (2.1)$$

where  $E \equiv |\mathbf{E}|$  and  $B \equiv |\mathbf{B}|$ .

This quantity also has an alternative, more useful interpretation: it is the ratio of the magnitude,  $|\mathbf{E} \times \mathbf{B}|/B^2$  of the  $\mathbf{E} \times \mathbf{B}$  drift speed, to one-half the mean thermal speed  $(8kT/\pi m)^{1/2}$  of the emitted electrons.

Our method of calculating escaping flux is as follows. For each of a sufficient number of values of  $\theta$  and  $\epsilon$ , we choose a large enough discrete set of values of emission velocity components  $v_{x0}$ ,  $v_{y0}$ , and  $v_{z0}$ ; we then search numerically along each of the resulting electron orbits, which are known analytically with time as a parameter, in order to determine which ones reimpact the surface. We then sum over the escaping ones to calculate the flux, and we tabulate the resulting flux values as a function of  $\theta$  and  $\epsilon$ . Further details of the calculation have been given by Laframboise (1985). The resulting values of escaping secondary-electron current density are shown in Fig. 4. These results are accurate to within about 0.5% or better (Laframboise, 1985). An empirical analytic expression which approximates these results to within 3% of  $I_0$  has been given by Laframboise (1985, Eq. 3.1).

An important feature of these results is that when  $\epsilon$  is large enough, electron escape becomes essentially complete except when  $\theta$  is very nearly  $90^\circ$ . This means that in Shuttle high-voltage charging conditions, for which  $30 \leq \epsilon \leq 120$  (Laframboise, 1985), the occurrence of high-voltage charging in marginal circumstances may depend very strongly on the precise orientation of a surface. A slowly-rotating surface which passes through tangentiality to  $\mathbf{B}$  may experience a sudden, brief high-voltage charging event. For the same reason, attempts to predict high-voltage charging may be afflicted by 'sensitivity' problems: if one attempts to predict worst-case charging by assuming that secondaries do not escape, then the resulting predictions are likely to be overly pessimistic most of the time. On the other hand, if one assumes that secondaries do escape, correct predictions will be obtained almost all of the time, but occasionally a large underestimate of charging will occur.

If a spacecraft surface is charged to a nonuniform potential, then  $E$  will have a nonzero component tangential to the surface. The resulting problem geometry is more complicated, and two additional angles,  $\alpha$  and  $\psi$ , which define the direction of  $-eE$ , need to be specified (Fig. 5). Calculations of escaping fluxes, and also the surface currents produced by reimpacting electrons, are in progress (J.G. Laframboise, to be published). Here we indicate only some general features which these results must possess.

It may happen that even though  $-eE$  points outward from the surface, its projection along  $B$  points inward (Fig. 6a). This will happen if the angle between  $-eE$  and  $B$  (or  $-B$ , if this points outward) is larger than  $90^\circ$ . In this case, every electron experiences an average acceleration toward the surface, and no electrons escape. This will greatly enlarge the range of surface orientations for which electron escape is strongly inhibited; when  $-eE$  was normal to the surface, Fig. 4 indicated that this range was a few degrees or less. The situation is analogous to that for a sailboat tacking against the wind (Fig. 6b).

The situation in which all electrons reimpact can be further subdivided (Fig. 7). The  $z$ -component of the  $E \times B$  drift direction is  $-B_x E_y / B^2$ . If  $B_x > 0$ , this is opposite in sign to  $E_y$ . Therefore, if  $E_y < 0$ , electrons which do not reimpact during the first gyroperiod after their emission are likely to travel much farther along the surface before they do reimpact, and the resulting surface current is likely to be much larger, than if  $E_y > 0$  (Fig. 7). Another consequence if  $E_y < 0$  is that electrons are more likely to travel distances across which our assumption of uniformity of  $E$  and  $B$  is no longer valid, and our detailed predictions will then become inaccurate.

### 3. ESTIMATE OF REQUIRED ENVIRONMENTAL CONDITIONS FOR LOW-POLAR-ORBIT CHARGING.

In this Section, we develop a simple rough estimate of the conditions necessary for high-voltage charging in low polar orbit, and we show that spacecraft surface potentials are likely to depend more strongly on the ratio of ambient flux of high-energy electrons to that of all ions than on any other applicable environmental parameter. To do this, we make the following approximations:

- (1) We assume that magnetic-field effects on charged-particle motion are negligible. This assumption should be acceptable for initial estimates because the gyroradii of ions and high-energy electrons are generally a few metres or larger, especially in a high-voltage sheath (Table 1), and collection of "cold" ( $\sim 0.1$  eV) ionospheric electrons by a negatively-charged spacecraft will be very small, so their density is well-approximated by a Boltzmann factor, independently of the presence of a magnetic field.
- (2) We assume that ambient high-energy electrons have an isotropic velocity distribution. Large departures from this have been observed in auroral-plasma conditions (W.J. Burke, 1984, private communication), but this should not seriously affect the type of rough estimate made here. Parks and Katz, 1981, and Katz and Parks, 1983, assumed both the ion and electron fluxes to be unidirectional; we discuss this point later in this Section.
- (3) We ignore secondary-electron emission; magnetic-field effects would tend to suppress this on some parts of the spacecraft in any case (Laframboise, 1983a, 1985; Sec. 2).
- (4) We assume that the spacecraft is a unipotential sphere, large compared to the typical ambient Debye length of  $\leq 1$  cm. We consider only overall charging of the spacecraft. This neglects the possibility that local high-voltage charging may occur, especially on surfaces in the spacecraft wake (Sec. 4).
- (5) We assume that both ions and electrons have double-Maxwellian velocity distributions, with the colder component in either case having a temperature of 0.1 eV, and the hotter 1 keV or larger. In the spacecraft reference frame, these are superposed on a drift velocity equal and opposite to the spacecraft velocity.
- (6) Ions are assumed to be either  $H^+$  or  $O^+$ .

Note that assumption (3) could cause a false prediction that high-voltage charging occurs, while assumption (4) could cause a false prediction that it does not. The effects of assumptions (1), (2), and (5) are less clear; these could conceivably either increase or decrease predicted surface potentials. With regard to (6), assuming that the ions are  $H^+$  results in maximum wake-filling by ions. If there are any electrically-isolated surfaces in the spacecraft wake, this would result in decreased surface potentials (magnitudes); assuming  $O^+$  gives the reverse.

Probably the most serious difficulty in formulating a theory for low-orbit charging is the prediction of ion collection on downstream surfaces. As mentioned in assumption (3) above, we avoid this difficulty by considering only total, rather than local, ion collection, on a unipotential sphere. Kanal [1962, Eq. (63)] gives an expression for the ion current collected by such a sphere from a drifting Maxwellian plasma in the limit of zero potentials (relative to space potential), as follows:

$$I_i = \frac{1}{2} \left[ \pi^{\frac{1}{2}} \left( S_i + \frac{1}{2S_i} \right) \operatorname{erf}(S_i) + \exp(-S_i^2) \right] \quad (3.1)$$

where  $I_i = I_i/I_{oi}$ ,  $I_{oi}$  is the ion random current  $e n_{i\infty} (kT_i/2\pi m_i)^{\frac{1}{2}}$ ,  $S_i = U/(2kT_i/m_i)^{\frac{1}{2}}$  is the ion speed ratio,  $U$  is the ion drift speed relative to the spacecraft,  $e$  is the magnitude of the electronic charge,  $k$  is Boltzmann's constant, and  $m_i$ ,  $T_i$ , and  $n_{i\infty}$  are ion mass, temperature, and ambient number density. We assume that  $U = 8$  km/sec, corresponding to low circular orbit.

We need to take account of the effect of a large ion-attracting surface potential on ion collection, in the limit of small Debye length  $\lambda_D$  compared to the sphere radius  $r_s$ . To do this, we use a result of Parrot et al (1982). These authors show that for a probe in a collisionless, nonmagnetized, Maxwellian plasma having  $T_i/T_e = 1$  and without ion drift, and in the limit when  $\lambda_D/r_s \rightarrow 0$  but  $-e\phi_s/kT \gg 1$  [where  $\phi_s$  is surface potential relative to space, and these limits must be approached in such a way that  $(-e\phi_s/kT)(\lambda_D/r_s)^{4/3}$  remains  $\ll 1$ , i.e., sheath thickness remains  $\ll$  sphere radius], the ion (attracted-particle) current is larger than the random current by a factor of 1.45. This factor represents the effect of "presheath" electric fields on ion collection. Even though several of their assumptions are unfulfilled in our case, the resulting effects on ion collection are probably small enough for our purposes. We therefore multiply Eq. (3.1) by the same factor to obtain an estimate of total ion collection as influenced by surface-potential effects. The resulting ion-current dependence on ion speed ratio is plotted in Fig. 8. For  $O^+$  ions at  $T = 0.1$  eV (1160K),  $H^+$  at 0.1 eV,  $O^+$  at 1keV, and  $H^+$  at 1keV, we have  $S_i = 7.31, 1.83, 0.0731$ , and  $0.0183$  (the latter two are effectively zero), respectively. The corresponding ion-current enhancement factors (values of  $I_i$ ) from Fig. 8 are 9.50, 2.69, 1.45, and 1.45, respectively.

If the ambient ions are  $H^+$ , the ion collected current is now given by:

$$I_i = 4\pi r_s^2 e n_{ic} \left\{ \frac{kT_{ic}}{2\pi m_i} \right\}^{\frac{1}{2}} \quad (2.69) \quad (3.2)$$

$$+ 4\pi r_s^2 e n_{ih} \left\{ \frac{kT_{ih}}{2\pi m_i} \right\}^{\frac{1}{2}} \quad (1.45)$$

where the subscripts  $ic$  and  $ih$  refer to the cold and hot ion populations. If the ions are  $O^+$ , then the factor 2.69 in (3.2) should be replaced by 9.50.

The electron collected current is:

$$I_e = 4\pi r_s^2 e n_{ec} \left\{ \frac{kT_{ec}}{2\pi m_e} \right\}^{\frac{1}{2}} \exp\left\{ \frac{e\phi_s}{kT_{ec}} \right\} + 4\pi r_s^2 e n_{eh} \left\{ \frac{kT_{eh}}{2\pi m_e} \right\}^{\frac{1}{2}} \exp\left\{ \frac{e\phi_s}{kT_{eh}} \right\}. \quad (3.3)$$

If high-voltage charging occurs, then  $-e\phi_s \gg kT_{ec}$ , and the first term on the right-hand side of this equation becomes negligible.

For current balance,  $I_i = I_e$ . This leads to:

$$2.69 n_{ic} \sqrt{T_{ic}} + 1.45 n_{ih} \sqrt{T_{ih}} = n_{eh} \sqrt{m_i/m_e} \sqrt{T_{eh}} e^{-e|\phi_s|/kT_{eh}} \quad (3.4)$$

where  $\sqrt{m_i/m_e} = 43$  for  $H^+$  ions. Therefore:

$$e|\phi_s|/kT_{eh} = \ln \left[ \frac{43n_{eh}\sqrt{T_{eh}}}{2.69n_{ic}\sqrt{T_{ic}} + 1.45n_{ih}\sqrt{T_{ih}}} \right] \quad (3.5)$$

for H<sup>+</sup> ions, with 43 and 2.69 replaced by 172 and 9.50 for O<sup>+</sup> ions. This is equivalent to:

$$e|\phi_s|/kT_{eh} = \ln \left[ \frac{\text{hot-electron ambient flux}}{2.69 (\text{cold-ion ambient flux}) + 1.45 (\text{hot-ion ambient flux})} \right] \quad (3.6)$$

For high-voltage charging to become probable, the argument of the ln function must be close to or larger than  $e \approx 2.72$ , i.e.:

$$\frac{\text{hot-electron ambient flux}}{2.69(\text{cold-ion ambient flux}) + 1.45(\text{hot-ion ambient flux})} \geq 2.72. \quad (3.7)$$

For O<sup>+</sup>/H<sup>+</sup> mixtures and for hot-ion temperatures other than 1 keV, generalization of this result is straightforward. Since any hot ions are likely to have  $T_{ih}/T_{ic} \approx 10^4$ , the hot-ion ambient flux will exceed the cold-ion ambient flux if the hot ions constitute more than about 1% of the total ambient-ion number density. Equation (3.7) indicates that the onset of high-voltage charging can be expected to depend primarily on the ratio of hot-electron ambient flux to the ambient flux of all ions, as mentioned at the beginning of this Section. This completes our argument in support of this conclusion.

In analyzing spacecraft data, one is therefore likely to find better correlation of spacecraft voltages with the ratio which appears in Eq. (2.3), or something nearly equal to it, than with any other measurable quantity, such as electron or ion density or average energy, taken individually. This expectation has been borne out in recent work by Gussenhoven et al (1985, Fig. 7), involving charging data from the DMSP F6 and F7 satellites. In calculating values of this ratio, the ambient fluxes which are involved need to have been measured simultaneously on the same spacecraft. Even though the approximations made in deriving (3.7) are severe, and the precise dependence of spacecraft voltages on this ratio may therefore differ substantially from that given in Eq. (3.7) (and the coefficients in (3.7) will need to be modified if O<sup>+</sup> dominates), our general conclusion, i.e. that spacecraft voltages should correlate most strongly with this ratio, or something nearly equal to it, is likely to remain valid. Furthermore, the dependence of spacecraft voltages on this flux ratio is likely to retain an approximately exponential form. In situations where most secondary and backscattered electrons emitted by the spacecraft will escape (see Sec. 2), primary-electron incident fluxes will be approximately cancelled for many spacecraft materials by electron escape at incident energies up to a few keV (Laframboise et al, 1982a,b; Laframboise and Kamitsuma, 1983; Lai et al, 1983), so the hot-electron ambient flux term in (3.7) needs to be modified accordingly.

The most serious approximation made in deriving (3.7) is probably item (4) in the list at the beginning of this Section. This is because ion fluxes on downstream surfaces are likely to be very much smaller than their average over the entire spacecraft. They are also likely to be strongly dependent on spacecraft geometry, local surface potential distribution, and O<sup>+</sup>/H<sup>+</sup> concentration ratio. Therefore, the critical value of ambient flux ratio, at which the onset of high-voltage charging occurs, is likely to vary substantially among spacecraft having different geometries and surface materials. In particular, for spacecraft having electrically-isolated downstream surfaces, this critical ratio is likely, because of local charging on these surfaces, to be much lower than for spacecraft which have an entirely conductive surface (Sec. 4).

Furthermore, in contrast with the situation for total ion collection, there is no known, simple, reliable method for estimating ion fluxes on downstream surfaces. Parks and Katz (1983a,b) have developed an ion flux calculation for the downstream point on a sphere in a potential which has a given, simple analytic form. Detailed numerical simulation, which includes realistic self-consistent spacecraft sheath potential distributions, and which probably needs to involve at least some ion orbit-following, therefore appears to be essential. In Sec. 4, we report on preliminary results from a calculation of this kind.

So far, we have not mentioned the difficulties which can arise in measuring the ambient ion fluxes which appear in Eq. (3.7). So far, we have also defined "ambient flux" to be that measured in an Earth-fixed reference frame. The alternative would be to define it as that measured in the spacecraft frame, i.e., including ram effects. Ion fluxes measured by spacecraft instruments are strongly influenced by ram effects. In fact, the numerical factors 2.69, 1.45, and 9.50, which appear in Eq. (3.7) and the associated discussion, already constitute a rough ram-effect correction, but for total current to a sphere, not for local collection by a forward-facing instrument aperture. It may happen that the ram-effect correction factors for an instrument are nearly equal to the above factors, so that the instrument measurement, without any correction, already gives a good estimate of the denominator of Eq. (3.7). In any case, the response of the instrument will depend on its geometry, and this problem has already been treated by other authors (Parker, 1970; Parker and Whipple, 1970; Whipple et al, 1974; Chang et al, 1979; Singh and Baugher, 1981; Comfort et al, 1982; Laframboise, 1983b), so we do not discuss it here.

Parks and Katz (1981) and Katz and Parks (1983) have estimated charging potentials on spherical spacecraft of 0.5m and 5m radius, assuming that the ions are  $O^+$ , the hot electron temperature  $T_{eh}$  is 5 keV, and spacecraft speed is 8 km/sec.

Their results can be compared directly with those given by our Eqs. (3.5) - (3.7). They have used the theory of Langmuir and Blodgett (1924) to obtain values for sheath radius as a function of spacecraft potential. They present spacecraft potentials as functions of the ratio  $\kappa$  of hot ("precipitating") electron ram current to ion ram current. To make a comparison, their value of  $\kappa$  needs to be expressed in terms of our ambient flux ratio. They have assumed the ambient electron flux to be unidirectional. To convert to an equivalent isotropic flux, we note that current to a sphere =  $4\pi r_s^2 \times$  isotropic (random) flux, but =  $\pi r_s^2 \times$  unidirectional (ram) flux.

Therefore, equivalent isotropic flux =  $\frac{1}{4} \times$  unidirectional flux, for a sphere.

Also for a sphere, the ratio of ion ram to random currents is  $U/(8kT_i/\pi n_i)^{1/2} = \frac{1}{2} \sqrt{\pi} S_i$ . Using  $S_i = 7.31$ , this ratio = 6.48, so therefore:

$$\begin{aligned} \text{their } \kappa &= \frac{\text{hot electron ram current}}{6.48 \times \text{total ion random current}} \\ &= \frac{\pi r_s^2 \times \text{hot electron ram flux}}{6.48 \times 4\pi r_s^2 \times \text{total ion random flux}} \quad (3.8) \\ &= \frac{1}{6.48} \times \frac{\text{hot electron (equivalent) random flux}}{\text{total ion random flux}} \\ &= \frac{1}{6.48} \times \text{our flux ratio } R. \end{aligned}$$

With coefficients for  $O^+$  used, our Eq. (3.6) gives:

$$\phi_s = -5000 \ln (R/9.50). \quad (3.9)$$

Figure 9 shows our result and theirs [from their Fig. 3 (1981) or Fig. 2 (1983)], plotted together. At larger potentials, the combined set of results shows a monotonic progression toward increased charging for larger spacecraft. For  $-\phi_s < 350V$ , their 5m sphere shows more charging than our large-radius-limit sphere. This is because their ion-current enhancement factor, which is determined by the size of a sharp-edged Langmuir-Blodgett sheath, falls below ours, which includes the effect of a quasineutral presheath. This discussion suggests that the tendency toward high-voltage charging always increases with spacecraft size, but magnetic-field effects may modify this (Laframboise, 1983a, Sec. 1). The corresponding curves for local charging, on surfaces in a spacecraft wake, will lie to the left of those shown in Fig. 9, but these remain to be computed numerically, as we have done for a particular spacecraft geometry in Sec. 4.

#### 4. RESULTS FROM A NUMERICAL SIMULATION

The simple treatment developed in Sec. 3 led to a suggestion that the onset of high voltage charging in low polar orbit can be expected to depend primarily on the ratio  $R$  of the hot-electron ambient flux to the ambient flux of all ions. In this Section we present preliminary results from numerical simulation work which is directed toward verifying this suggestion. This work uses an adaptation of a previously-existing simulation program written by one of us (Parker, 1983) for an infinite-cylindrical spacecraft geometry in a collisionless plasma crossflow. If the spacecraft surface is entirely dielectric, then at progressively increasing values of  $R$ , one might expect surfaces in the spacecraft wake to be the first to undergo high-voltage charging, followed by sideways-facing and finally frontward-facing surfaces, as shown schematically in Fig. 10. The numerical results show that at least one implied feature of Fig. 10, namely the apparent monotonic progression to larger negative voltages as one moves around the surface of the cylinder toward the wake point, is wrong; we will return to this question later.

Our simulation geometry is shown in Fig. 11. Our original intention was to model a completely dielectric cylinder, but we have substituted a set of electrically-isolated conductive sectors in the wake region because we found that strong ion focusing effects occurred in the wake, and these produced very localized ion-current deposition regions or "ion hot spots", whose location was very sensitive to small variations which occurred in the sheath potential distribution as iteration proceeded toward a self-consistent set of surface potentials. Averaging these ion currents over the  $10^\circ$  or  $20^\circ$  intervals shown in Fig. 11 suppressed the resulting instabilities and allowed the iterative procedure to converge. The parameter values chosen for this study included: Debye length  $\lambda_D$ /spacecraft radius  $r_s = 0.001$ , ion speed ratio  $S_i$  ( $=$  drift speed  $U$ /ion most-probable thermal speed  $\sqrt{2kT_i/m_i}$ )  $= 8$ , ions  $O^+$  at a temperature of 0.2 eV, cold electrons at 0.2 eV, and hot (auroral) electrons at 5 keV. We have again made the assumptions (1), (2), and (3) listed in Sec. 3.

The discretization used for position space is indicated in Fig. 11. "Inside-out" ion orbit-following was used for calculating ion surface current densities. The ion velocity-space discretization used was similar to that described by Parker (1977). To achieve sufficient accuracy in ion flux values at wake-side surface points required use of 1024 incident ion directions at each of 32 ion energy levels at each such point. The iteration was started using an ion density distribution based on assuming that ions behaved as neutrals, and iterating until the surface potential, surface ion current density, sheath potential and sheath electron density distributions all converged. Electron densities and currents were described by superpositions of Boltzmann factors. Each such calculation took about 6 hours on the AFGL Cyber 850. The next intended step was to calculate an ion density distribution corresponding to the resulting sheath potential distribution, then "freeze" this ion density distribution and iterate the other quantities involved as before, and so on. Each such step would take about 24 hours on the same computer, so we have not so far made such calculations, and the results presented here are therefore based on the "neutral approximation" for ion densities, but on ion orbit-following for ion current collection on surfaces. Further details of the calculation method are to be published in a later paper (Laframboise and Parker, to be published).

Preliminary results from these calculations are shown in Fig. 12, for flux ratios  $R = 0.1, 0.25, 0.5,$  and  $5.0$ . On the front and sides of the cylinder ( $\theta \leq 100^\circ$ ), surface potentials seem to increase more-or-less monotonically as one moves away from the front ( $\theta = 0^\circ$ ), except for some relatively small oscillations which are probably spurious, and may be caused either by two coarse a position-space discretization, incomplete convergence, or insufficiently fine sampling of the ion velocity space (even with 32,768 orbits followed per surface point, very few of these will connect back to the ambient plasma with an ambient velocity close to that of the heavily-populated part of the ion distribution).

However, on rearward surfaces ( $\theta \geq 110^\circ$ ), there is some non-monotonicity which appears to be real. For  $R = 0.1, 0.25,$  and  $0.5$ , there are three surface-potential maxima, one at the rearmost point ( $\theta = 180^\circ$ ) and one on each side of it. For  $R = 0.1$  and  $0.25$ , these features were almost unchanged (the potentials of the maxima changed by less than 2%) when as few as 4,096 ion orbits (4 ion energy levels) were used, and this attests to their reality. For  $R = 5$ , we obtain four maxima, two on either side of the rearmost point. The minima between these peaks correspond to the ion "hot spots", or deposition points of highly beam-like ion populations, mentioned above. Most real situations would not possess the symmetry about the fore-aft line which our problem does, but our results nonetheless indicate that high-voltage wake regions of spacecraft are likely to contain very beam-like ion population components generally.

This is related also to the fact that the ambient ion distribution is a highly-directed ( $S_1 = 8$ ) one. A situation with ion drift is very different than one without. A drifting distribution is not an equilibrium one. The drift provides the ions with thermodynamic free energy which can support a much greater variety of phenomena than in the nondrifting case, including self-excited oscillations (Krall and Trivelpiece, 1973, Chs. 2 and 9). For related reasons, the drift also makes possible ion focusing effects including those discussed here. In the steady-state treatment described here, self-excited oscillations cannot be treated. However, oscillations recently observed in the outer portions of the Shuttle wake involve density fluctuations of only a few per cent (Murphy, 1985), so they probably do not have much effect on the steady-state wake properties studied here.

Beam-like ion components have important implications for more complicated situations, such as the interior of the Shuttle's cargo bay. As our work has indicated, beam impact points will be very sensitive to details of the potential distribution on or near a spacecraft. Ions may come around a corner of the spacecraft, just miss one equipment box, and impact on one small corner of the next box, which may then come to a potential very different than those of its surroundings.

In addition, more than one ion beam may be present at some points in the sheath. Beams may come around corners from opposite sides of a spacecraft, and beams may also be present which have circled the spacecraft one or more times. Ion distributions as a function of angle may therefore contain many narrow "peaks" and "valleys". Simulation of a very detailed kind, demanding the maximum available computer power, will be necessary to resolve such situations.

In Fig. 9, we have also plotted the largest value of negative surface potential for each of the four values of  $R$  shown in Fig. 12, for comparison with our simple prediction from Sec. 3. These values are shown as circled points in this Figure. These results qualitatively resemble the theoretical curves in the same Figure, and also our expected behaviour shown in Fig. 10, in that they appear to show almost no dependence on  $R$  until a "threshold" value is reached, and then they show a rapid increase. Furthermore, this increase appears to begin at a substantially lower  $R$  value than for these curves, as one expects since the curves are for whole-body charging and the plotted points are for charging of electrically-isolated surfaces in the wake.

One feature of these results is unexpected: the "pre-threshold" wake charging, instead of being close to zero, is already several hundred volts. However, this apparent threshold is not the true one. High-voltage charging conventionally means that surface potential exceeds 100V in magnitude. For our conditions, and for a surface potential of -100V, the hot-electron flux exceeds the cold electron flux when  $R > 1.2 \times 10^{-22.5}$ . Also, for  $R = 0.1$  (the left margin of Fig. 9), if we calculate downstream-point potential using the neutral approximation for ion flux (Tsien, 1946; Parks and Katz, 1983b, Eq. 4), we obtain  $\phi_s = -3.3 \times 10^5$ V. For  $R = 0$  (cold electrons only), a similar calculation yields  $\phi_s = -14.8$ V. It is evident that all the numerical simulation results shown in Fig. 9 are "post-threshold" in the sense that they involve a current balance primarily between the hot electron flux and wake-region ion fluxes that are already heavily modified by orbit curvature in strong wake-region electric fields. This is evidently a situation in which even a small amount of ambient  $H^+$  can be expected to produce a large decrease in wake-region potentials, and we intend to include  $H^+$  effects in future calculations.

## REFERENCES

- Al'pert, Ya.L., Gurevich, A.V., and Pitaevskii, L.P. (1965), *Space Physics with Artificial Satellites*. Consultants Bureau, New York.
- Chang, J-S., Godard, R., and Laframboise, J.G. (1979), Mass-discrimination in ion and neutral extraction by mass-spectrometers under spacecraft conditions. *Planet. Space Sci.* 27, 1213-1220.
- Comfort, R.H., Baugher, C.R., and Chappell, C.R. (1982), Use of the thin sheath approximation for obtaining ion temperatures from the ISEE 1 limited aperture RPA, *J. Geophys. Res.* 87 (A7), 5109-5123.
- de Leeuw, J.H. (1967), A brief introduction to ionospheric aerodynamics. In: *Proc. Fifth Internat. Symp. on Rarefied Gas Dynamics*, edited by C.L. Brundin, Academic Press, New York, pp. 1561-1586.
- Gussenhoven, M.S., Hardy, D.A., Rich, F., and Burke, W.J. (1985), High-level spacecraft charging in the low-altitude polar auroral environment. *J. Geophys. Res.* 90 (A11), 11009-11023.
- Kanal, M. (1962), Theory of current collection of moving spherical probes. *Space Physics Research Lab., University of Michigan, Ann Arbor*, report JS-5.
- Katz, I., and Parks, D.E. (1983), Space shuttle orbiter charging. *J. Spacecraft and Rockets* 20, 22-25.
- Krall, N.A., and Trivelpiece, A.W. (1973), *Principles of Plasma Physics*. McGraw-Hill, New York.
- Laframboise, J.G. (1983a), Is there a good way to model spacecraft charging in the presence of space charge coupling, flow, and magnetic field? In: *Proc. Air Force Geophys. Lab. Workshop on Natural Charging of Large Space Structures in Near Earth Polar Orbit*, edited by R.C. Sagalyn, D.E. Donatelli, and I. Michael, Report No. AFGL-TR-83-0046/Environmental Research Paper No. 825, Air Force Geophysics Laboratory, Massachusetts, pp. 57-78. ADA134894
- Laframboise, J.G. (1983b), Incident velocity distributions on sampling electrodes of spacecraft plasma instruments. In: *Proc. 17th ESLAB Symposium on "Spacecraft/Plasma Interactions and their Influence on Field and Particle Measurements"*, Report No. ESA SP-198, European Space Agency Scientific and Technical Publications Branch, ESTEC, Noordwijk, The Netherlands, pp. 101-108.
- Laframboise, J.G. (1985), Calculation of secondary-electron escape currents from inclined spacecraft surfaces in a magnetic field. In: *Spacecraft Environmental Interactions Technology 1983*, edited by C.K. Purvis and C.P. Pike, NASA Conference Publication 2359/Report No. AFGL-TR-85-0018, Air Force Geophysics Laboratory, Massachusetts, pp. 277-286.
- Laframboise, J.G., Kamitsuma, M., and Godard, R. (1982a), Multiple floating potentials, "threshold-temperature" effects, and "barrier" effects in high-voltage charging of exposed surfaces on spacecraft. In: *Proc. Internat. Symp. on Spacecraft Materials in Space Environment, June 1982, Toulouse, France*, European Space Agency, Paris, Publication no. ESA SP-178, pp. 269-275.
- Laframboise, J.G., Kamitsuma, M., Prokopenko, S.M.L., Chang, Jen-Shih and Godard, R. (1982b), Numerical simulation of spacecraft charging phenomena at high altitude, Final Report on Grant AFOSR-76-2962, York University.
- Laframboise, J.G., and Kamitsuma, M. (1983), The threshold temperature effect in high-voltage spacecraft charging. In: *Proc. Air Force Geophys. Lab. Workshop on Natural Charging of Large Space Structures in Near Earth Polar Orbit*, edited by R.C. Sagalyn, D.E. Donatelli, and I. Michael, Report No. AFGL-TR-83-0046/Environmental Research Paper No. 825, Air Force Geophysics Laboratory, Massachusetts, pp. 293-308. ADA134894
- Lai, S.T., Gussenhoven, M.S., Cohen, H.A. (1983), The concepts of critical temperature and energy cutoff of ambient electrons in high voltage charging of spacecraft. In: *Proc. 17th ESLAB Symposium on "Spacecraft/Plasma Interactions and their Influence on Field and Particle Measurements"*, Report No. ESA SP-198, European Space Agency Scientific and Technical Publications Branch, ESTEC, Noordwijk, The Netherlands, pp. 169-175.
- Langmuir, I., and Blodgett, K.B. (1924), Currents limited by space charge between concentric spheres. *Phys. Rev.* 23, 49.

- Martin, A.K., (1974), Numerical solutions to the problem of charged particle flow around an ionospheric spacecraft. *Planet Space Sci.* 22, 121-141.
- Murphy, G.B. (1985), Electromagnetic environment of the Orbiter at S-band and Ku-band frequencies. Paper A1AA-85-7036-CP, AIAA Shuttle Environment and Operations II Conference, Houston, 11-13 Nov. 1985.
- Parker, L.W. (1970), Theory of the external sheath structure and ion collection characteristics of a rocket-borne mass spectrometer, Report No. AFCRL-71-0105, Air Force Geophysics Laboratory, Hanscom AFB, Massachusetts, U.S.A. AD720131
- Parker, L.W. (1977), Calculation of sheath and wake structure about a pillbox-shaped spacecraft in a flowing plasma. In: Proc. Spacecraft Charging Technology Conf., edited by C.P. Pike and R.R. Lovell, Report No. AFGL-TR-77-0051, Air Force Geophysics Laboratory, Massachusetts/NASA TMX-73537, Lewis Research Center, Cleveland, pp. 331-366. ADA045459
- Parker, L.W. (1983), Contributions to satellite sheath and wake modeling. In: Proc. 17th ESLAB Symposium on "Spacecraft/Plasma Interactions and their Influence on Field and Particle Measurements", Report No. ESA SP-198, European Space Agency Scientific and Technical Publications Branch, ESTEC, Noordwijk, The Netherlands, pp. 81-100.
- Parker, L.W. and Whipple, E.C. Jr. (1970), Theory of spacecraft sheath structure, potential, and velocity effects on ion measurements by traps and mass spectrometers, *J. Geophys. Res.* 75, 4720-4733.
- Parks, D.E., and Katz, I. (1981), Charging of a large object in low polar Earth orbit. In: *Spacecraft Charging Technology 1980*, NASA Conference Publication 2181/Report No. AFGL-TR-81-0270, Air Force Geophysics Laboratory, Massachusetts, pp. 979-989. ADA114426
- Parks, D.E., and Katz, I. (1983a), Electric field effects on ion currents in satellite wakes. In: *Spacecraft Environmental Interactions Technology 1983*, edited by C.K. Purvis and C.P. Pike, NASA Conference Publication 2359/Report No. AFGL-TR-85-0018, Air Force Geophysics Laboratory, Massachusetts, pp. 195-204.
- Parks, D.E., and Katz, I. (1983b), Mechanisms that limit potentials on ionospheric satellites. *J. Geophys. Res.* 88, 9155-9162.
- Parrot, M.J.M., Storey, L.R.O., Parker, L.W., and Laframboise, J.G. (1982), Theory of cylindrical and spherical Langmuir probes in the limit of vanishing Debye number. *Physics of Fluids* 25, 2388-2400.
- Singh, N., and Baugher, C.R. (1981), Sheath effects on current collection by particle detectors with narrow acceptance angles. *Space Sci. Instrum.* 5, 295-305.
- Tsien, H.-S. (1946), Superaerodynamics, mechanics of rarefied gases. *J. Aeronaut. Sci.* 13, 653-664.
- Whipple, E.C., Warnock, J.M. and Winkler, R.H. (1974), Effects of satellite potential on direct ion density measurements through the plasmopause. *J. Geophys. Res.* 79, 179-186.

#### ACKNOWLEDGMENTS

This work was supported by the U.S. Air Force Geophysics Laboratory under Contract No. F19628-83-K-0028.

TABLE 1. Low-Earth-Orbit Conditions\*\*

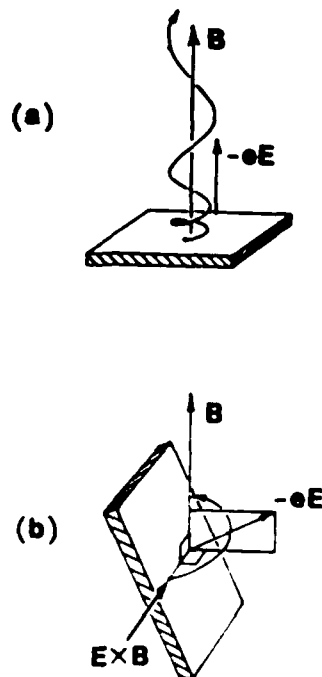
<b>(a) CHARACTERISTIC LENGTHS</b>		
Ambient Debye Length:		$\leq 1$ cm
Thickness of 1kV and 5kV spherically-symmetric sheath*** around a sphere of radius 3m:		2.5m and 5.8m
Thickness of 1kV and 5kV planar Child-Langmuir sheath:		5.0m and 17m (WHY SO LARGE?)
Particle gyroradii:		
ambient electrons (0.1 eV)	2 cm	
secondary electrons (3 eV)	13 cm	
auroral electrons (10 keV)	8 m	
ions (0*; 0.1 eV)	3m in "rest" frame	
	27 m* in spacecraft frame	(larger inside a high-voltage sheath)
<b>(b) CHARACTERISTIC SPEEDS:</b>		
Ion thermal speed:	1 km/sec	} SITUATION IS "MESOTHERMAL"
Spacecraft speed:	$\leq 8$ km/sec, depending on orbit	
Electron thermal speed:	100 km/sec, for ambient electrons	

\* Particle motions do not depend on the frame of reference in which they are viewed. The transformation from rest frame to spacecraft frame produces a  $\mathbf{V} \times \mathbf{B}$  electric field  $\leq 0.35\text{V/m}$  where  $\mathbf{V}$  = spacecraft velocity and  $\mathbf{B}$  = magnetic induction; electric fields inside a 1kV sheath are  $\sim 200$  V/m.

\*\* deLeeuw (1967), p. 1564; Martin (1974).

\*\*\* Al'pert et al (1965), Fig. 72.

Figure 1. Effect of surface orientation on escape of emitted electrons. In (a), the spacecraft surface is perpendicular to the magnetic field  $\mathbf{B}$ , and the emitted electrons, which experience an electric force  $-e\mathbf{E}$  directed away from the surface, all escape. In (b), the spacecraft surface is nearly parallel to  $\mathbf{B}$ , and almost all of the emitted electrons return to the surface, even though they still experience an electric force directed away from it. Note that the component of  $\mathbf{E}$  perpendicular to  $\mathbf{B}$  results only in an  $\mathbf{E} \times \mathbf{B}$  drift parallel to the surface.



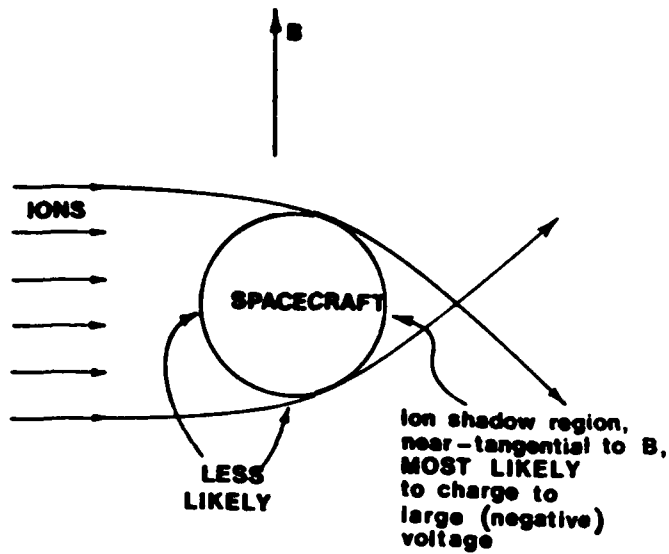


Figure 2. Spacecraft simultaneously in a collisionless ion flow and a magnetic field  $B$ .

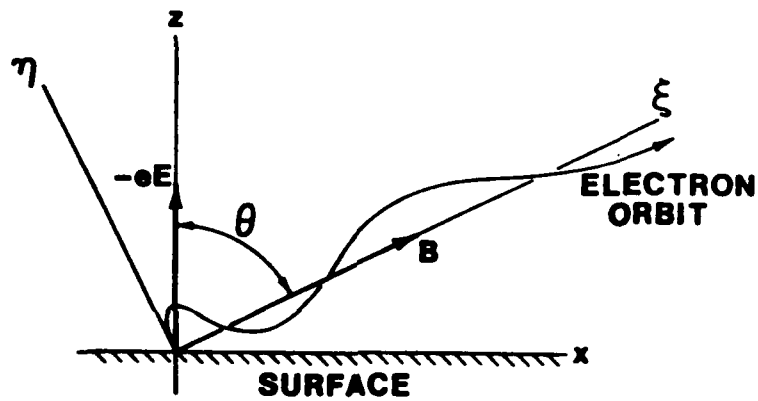
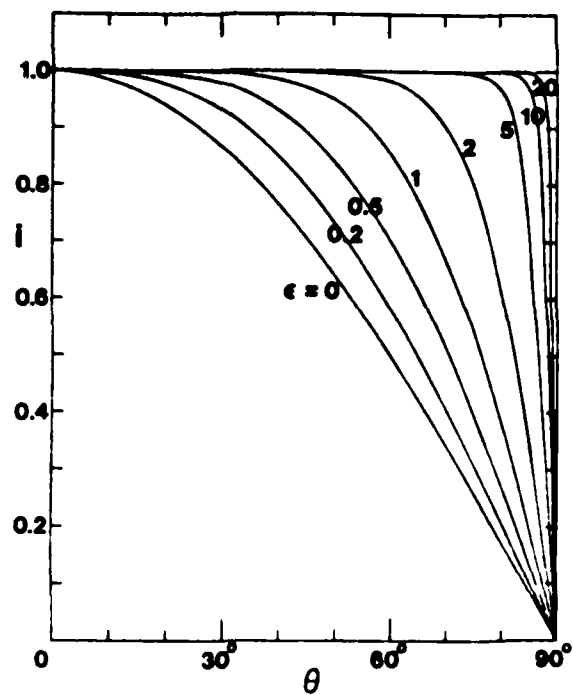


Figure 3. Coordinate system for calculating electron escape fluxes when  $E$  is perpendicular to the spacecraft surface. The  $y$ -coordinate (not shown) is directed into the plane of the Figure.

Figure 4. Ratio  $i = I/I_0$  of escaping to emitted secondary-electron flux, as a function of the angle  $\theta$  between the surface normal and the magnetic field direction, for various values of the repelling electric field strength parameter  $\epsilon = (E/B)(\pi m/2kT)^{1/2}$ . The result for  $\epsilon = 0$  is given by  $i = \cos \theta$ . Realistic values of  $\epsilon$  for Shuttle high-voltage charging conditions are in the range  $30 \leq \epsilon \leq 120$  (Laframboise, 1985)!



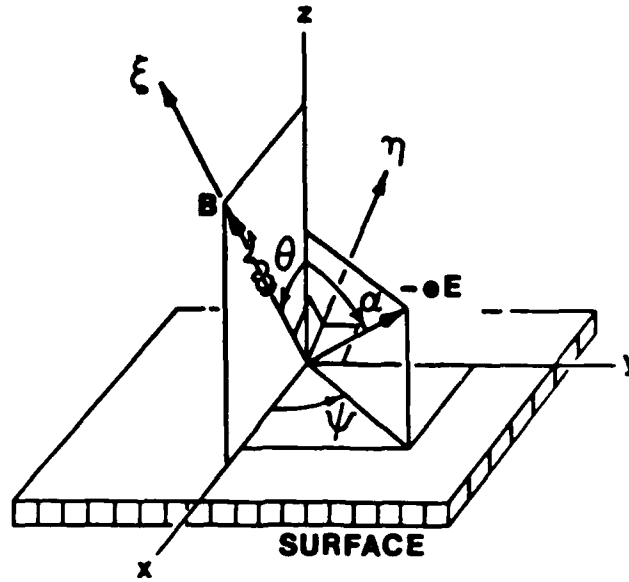


Figure 5. Problem geometry when potential also varies along surface.

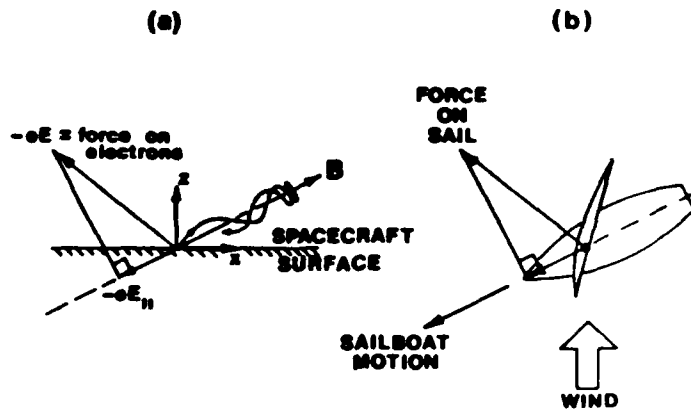


Figure 6. (a) Typical orbit of emitted electron when the electric force  $-eE$  on it has an outward normal component, but the projection of  $-eE$  along  $B$  has an inward normal component (b) analogous situation involving sailboat tacking into wind.

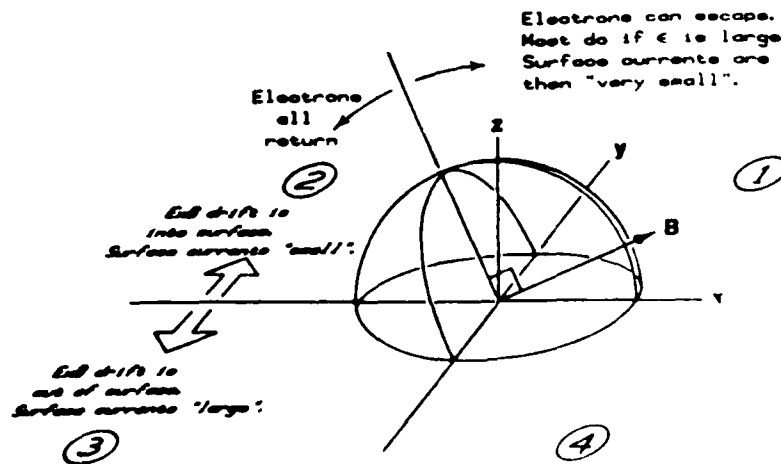


Figure 7. Dependence of secondary-electron escape and surface currents on electric field direction at surface.

Figure 8. Dependence of ion current to a sphere on ion speed ratio.

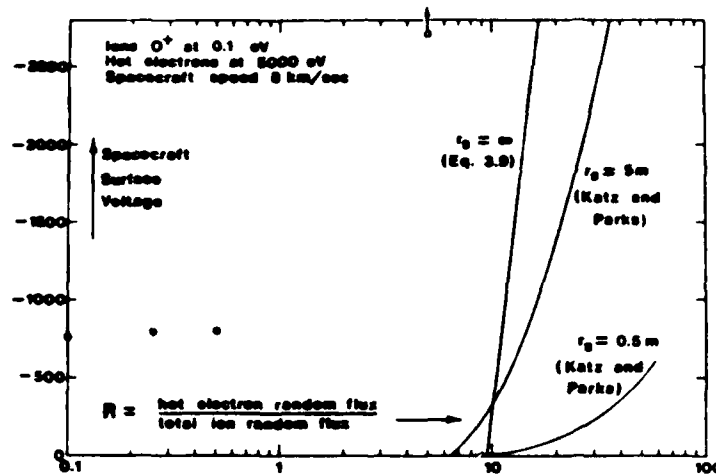
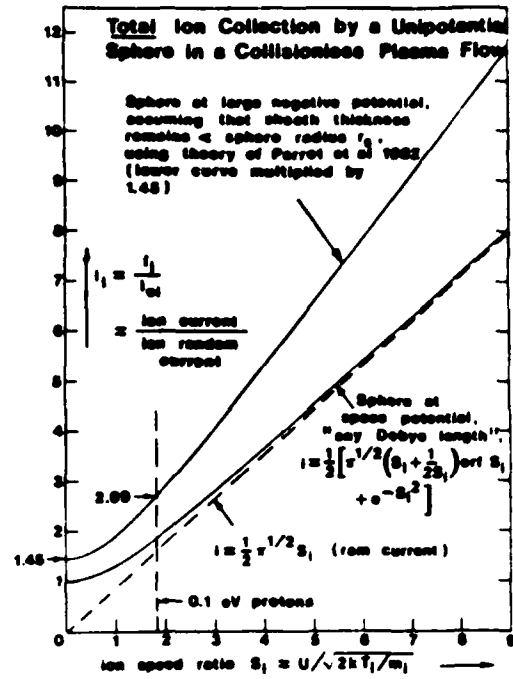


Figure 9. Dependence of spacecraft surface potential on hot electron/total ambient flux ratio. The four circled points are the largest values of surface potential from the numerical solutions discussed in Sec. 4 and presented in Fig. 12.

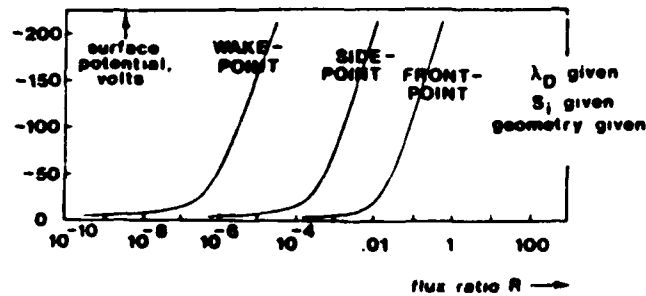


Figure 10. Expected general appearance of graphs of spacecraft surface potential as functions of ambient hot electron to total ion flux ratio  $R$ .

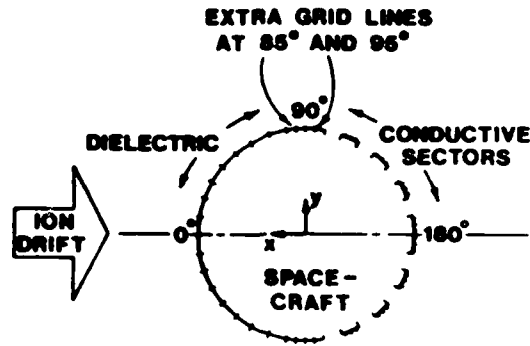


Figure 11. Geometry of simulated spacecraft used for computational purposes. The outer boundary of the computational domain is a square whose sides are at  $x = \pm 5r_s$ ,  $y = \pm 5r_s$ , where  $r_s$  is the spacecraft radius. The domain is covered by a finite-element grid in which there are 10 intervals along each radial line from the spacecraft surface to the outer boundary, and the size of these intervals is proportional to the radius. Within the gaps between the conductive sectors, the potential is assumed to vary linearly with surface position on the cylinder. The dots on the conductive sectors indicate locations on them where ion currents are calculated.

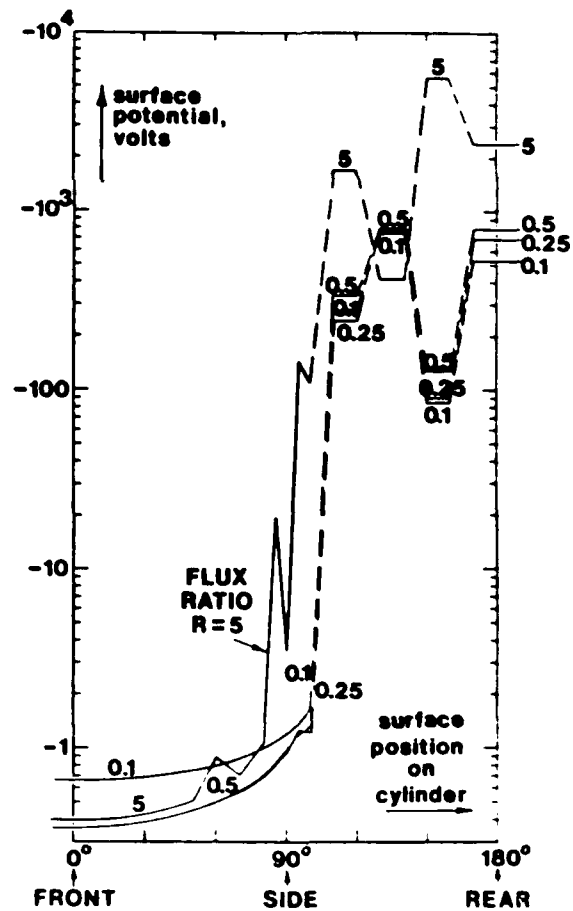


Figure 12. Surface potentials as functions of position for the spacecraft geometry shown in Fig. 11, for ratios R of hot electron to total ion ambient flux as shown.

CALCULATION OF SECONDARY-ELECTRON ESCAPE CURRENTS  
FROM NEGATIVELY-CHARGED SPACECRAFT SURFACES IN A MAGNETIC  
FIELD

J. G. Laframboise

Physics Department, York University

Toronto, Canada M3J 1P3

## ABSTRACT

In low Earth orbit, the geomagnetic field  $\mathbf{B}$  is strong enough that secondary electrons emitted from spacecraft surfaces have an average gyroradius much smaller than typical dimensions of large spacecraft. This implies that escape of secondaries will be strongly inhibited on surfaces which are nearly parallel to  $\mathbf{B}$ , even if a repelling electric field exists outside them. This effect is likely to make an important contribution to the current balance and hence the equilibrium potential of such surfaces, making high-voltage charging of them more likely. We present numerically-calculated escaping secondary electron fluxes for these conditions. For use in numerical spacecraft-charging simulations, we also present an analytic curve-fit to the results for the important case of normal electric field (uniformly-charged surfaces). This curve-fit is accurate to within 3% of the emitted current. For strong normal electric fields, escape is effectively suppressed only when a surface is parallel to  $\mathbf{B}$  within a few degrees or less, and this leads to "sensitivity effects" in attempts to predict auroral-zone spacecraft charging. A nonzero tangential component in the surface electric field can greatly enlarge the range of surface orientations for which escape is suppressed, and can also produce large surface currents.

## 1. INTRODUCTION

The prediction of high-voltage charging or other environmental effects on a spacecraft in low Earth orbit appears likely to be more complicated than in geostationary orbit, for at least three reasons.

These reasons are: (a) space charge effects (on sheath and wake potentials) are more important, because space-charge densities are much higher (the Debye length is no longer  $\gg$  typical spacecraft dimensions) (b) ion flow effects are more important, because spacecraft orbital speed  $\gtrsim$  ion thermal speeds (c) the geomagnetic field  $\mathbf{B}$  is likely to have an important influence on charged-particle motions because  $\mathbf{B}$  is now much larger, and not all of the average particle gyroradii of importance are any longer  $\gg$  typical spacecraft dimensions.

We wish to investigate an important consequence of (c), which concerns the escape of secondary electrons emitted from spacecraft surfaces. Our discussion will also apply, with minor modifications, to photoelectron or backscattered-electron escape. In low Earth orbit, in the auroral-zone geomagnetic field ( $|\mathbf{B}| = 0.44$  gauss  $= 4.4 \times 10^{-5}$ T), the gyroradius of a "typical" 3eV secondary electron and a 10 keV auroral electron are 13 cm and 8 m, respectively. The average gyroradius of "cold" ionospheric electrons (temperature  $T = 0.1$  eV) in the same  $\mathbf{B}$  is even smaller (2 cm), but this is not an important parameter in most cases because these electrons are repelled if the spacecraft potential is negative, and their density is then well-approximated by a Boltzmann factor, which is unaltered by  $\mathbf{B}$  effects.

The reason why  $\mathbf{B}$  affects secondary-electron escape is shown in Fig. 1. In Fig. 1(a), the spacecraft surface is perpendicular to  $\mathbf{B}$ , and the emitted electrons, which experience an electric force  $-e\mathbf{E}$  directed away from the surface, all escape, helping to discharge it. In Fig. 1(b), the spacecraft surface is nearly parallel to  $\mathbf{B}$ , and almost all of the emitted electrons return to it, even though they still experience an electric force directed away from it. These electrons therefore are unable to help discharge it, so a surface nearly parallel to  $\mathbf{B}$  is more likely to charge to a large negative voltage. Note that the component of  $\mathbf{E}$  which is perpendicular to  $\mathbf{B}$  results only in an  $\mathbf{E} \times \mathbf{B}$  drift parallel to the surface.

For any object much larger than 13 cm, the escape of secondary electrons will be strongly affected by this process. For example, most surfaces on the Shuttle are effectively "infinite planes" by this criterion. On the other hand, the average gyroradius of high-energy auroral electrons is comparable to Shuttle dimensions, so the deposition of these electrons onto Shuttle surfaces is likely to be only moderately inhibited.

For a larger object (size  $\gg 8$  m), deposition of auroral electrons will also become strongly orientation-dependent, with both collection and escape of electrons now being inhibited on surfaces nearly parallel to  $\mathbf{B}$ . This suggests that high-voltage charging of such surfaces may be more likely on objects of intermediate size than on either larger or smaller ones. In the calculation of Parks and Katz (1981), Katz and Parks (1983), the tendency toward high-voltage charging increased with spacecraft size because in their model,

ion collection increased less rapidly with spacecraft size than did electron collection. To determine which of these two effects predominates will require more detailed calculations than have been done so far.

As already mentioned, strong ion flow effects also are generally present in low orbit; the ion speed ratios (flow speed/most probable ion thermal speed) for  $H^+$  at 1 keV,  $H^+$  at 0.1 eV, and  $O^+$  at 0.1 eV are 0.02, 1.8, and 7.3, respectively. Whenever the latter is the predominant ion species, ion collection on downstream surfaces will therefore be strongly inhibited. If a surface is simultaneously downstream and nearly parallel to  $B$ , as is likely to be the case in the auroral zones, then the tendency for high-voltage charging to occur on it will be greatly increased (Fig. 2).

To "straightforwardly" include  $B$  effects on secondary electron emission in a large two or three dimensional simulation program would involve the numerical integration of very large numbers of secondary-electron orbits. The resulting computing costs usually would be formidable, especially since these orbits would have relatively large curvatures. A desirable alternative is to "parameterize" the situation by treating in advance a simplified but still sufficiently realistic model problem. In order to do this, we make the approximations described in the next Section.

## 2. THEORY FOR E NORMAL TO SURFACE

We assume that the spacecraft surface is an infinite plane, and the electric and magnetic fields  $\mathbf{E}$  and  $\mathbf{B}$  outside it are uniform. In this Section, we also assume that the electric force  $-e\mathbf{E}$  on electrons is directed along the outward normal to the surface; here  $e$  is the magnitude of the elementary charge. This assumption is relaxed in Sec. 4, in order to permit variations of potential along the surface to be taken into account. We assume that the secondary electrons are emitted with a Maxwellian distribution corresponding to a temperature  $T$ . The ratio  $i = I/I_0$  of escaping to emitted flux is then a function of two parameters: the angle  $\theta$  between the surface normal and the direction of  $\mathbf{B}$  (Fig. 3), and a parameter describing the strength of  $\mathbf{E}$ . A convenient choice for this parameter is the difference in potential across a mean secondary-electron gyroradius  $\bar{a} = (1/eB)(\pi mkT/2)^{1/2}$ , divided by  $kT/e$ , where  $m$  is electron mass and  $k$  is Boltzmann's constant.

This quotient is:

$$\epsilon \equiv \frac{E}{B} \sqrt{\frac{\pi m}{2kT}} \quad (2.1)$$

where  $E \equiv |\mathbf{E}|$  and  $B \equiv |\mathbf{B}|$ .

This quantity also has an alternative, more useful interpretation: it is the ratio of the magnitude  $|\mathbf{E} \times \mathbf{B}|/B^2$  of the  $\mathbf{E} \times \mathbf{B}$  drift speed, to one-half the

mean thermal speed  $(8kT/\pi m)^{1/2}$  of the emitted electrons. It is useful to estimate the value of  $\epsilon$  for a high-voltage spacecraft sheath in low-orbit conditions. To do this, we use the sheath solution of Al'pert et al (1965, Table XXIV and Fig. 72). For a 1 kV and a 5 kV sheath around a sphere of radius 3m in a collisionless plasma having an ambient ion temperature of 0.1 eV, number density of  $3 \times 10^5 \text{ cm}^{-3}$ , and resultant (ion) Debye length of 0.43 cm, their results give, respectively, sheath thicknesses of 2.6 and 6.1 m, and surface electric fields  $E = 0.86$  and  $2.9 \text{ kV/m}$ . Using  $B = 4.4 \times 10^{-5} \text{ T}$  and  $T = 3 \text{ eV}$  for secondary electrons, we then obtain  $\epsilon = 33.9$  and  $114.2$ . Both of these are relatively large values, whose significance can be understood if we consider what would happen if  $\epsilon$  were infinite.

In this limit, it is easy to show that secondary electrons would all escape unless  $\mathbf{B}$  were exactly parallel to the surface ( $\theta$  were  $90^\circ$ ). This can be shown as follows. In this limit, secondary electrons would have no "thermal" motion. The (y,z) projection of their motion would then be similar to that shown in Fig. 4. This motion would be the sum of: (i) an  $\mathbf{E} \times \mathbf{B}$  drift in the y direction (ii) a uniform acceleration along  $\mathbf{B}$ , whose projection in the (y,z) plane would be upward (iii) just enough gyromotion to produce a cycloidal path when combined with (i), so that in the absence of (ii), the electron would (just) return to the surface at the end of each gyroperiod. In the presence of (ii), these "return points" are displaced upward by progressively increasing amounts (Fig. 4), so the electron can never return to the surface, unless  $\mathbf{B}$  is exactly parallel to the surface, so that the upward component of  $-e\mathbf{E}$  along  $\mathbf{B}$  vanishes.

This result suggests that for large finite values of  $\epsilon$  (including the values

calculated above), electron escape is likely to be almost complete except for  $\theta$  very near  $90^\circ$ , where it should drop to zero very steeply. The occurrence of high-voltage charging in marginal circumstances may therefore depend very strongly on the precise orientation of a surface.

The escaping secondary-electron flux is given by:

$$\begin{aligned}
 I &= \iiint f(\mathbf{v}_0) H(\mathbf{v}_0) v_{0z} d^3\mathbf{v}_0 \\
 &= \int_{-\infty}^{\infty} dv_{0x} \int_{-\infty}^{\infty} dv_{0y} \int_0^{\infty} n \left\{ \frac{m}{2\pi kT} \right\}^{3/2} \exp\left\{ -\frac{mv_0^2}{2kT} \right\} H(v_{0x}, v_{0y}, v_{0z}) v_{0z} dv_{0z}
 \end{aligned}
 \tag{2.2}$$

where:  $\mathbf{v}_0$  is the initial velocity of an emitted electron,  $f(\mathbf{v}_0) \equiv d^3n/d^3\mathbf{v}_0$  is the velocity distribution of emitted electrons,  $n$  is a reference number density, and  $H(\mathbf{v}_0)$  is equal to 1 for escaping electrons and 0 for those which return to the surface. The emitted flux is:

$$I_0 = n(kT/2\pi m)^{1/2}.
 \tag{2.3}$$

We also introduce the dimensionless velocity:

$$\mathbf{u} = \mathbf{v} (m/2kT)^{1/2}.
 \tag{2.4}$$

Equation (2.2) then becomes:

$$\frac{I}{I_0} = \frac{2}{\pi} \int_{-\infty}^{\infty} \int_{-\infty}^{\infty} du_{0x} du_{0y} e^{-u_{0x}^2 - u_{0y}^2} \int_0^{\infty} du_{0z} u_{0z} e^{-u_{0z}^2} H(u_{0x}, u_{0y}, u_{0z})$$

$$\begin{aligned}
&= \frac{1}{\pi} \int_{-\infty}^{\infty} \int_{-\infty}^{\infty} du_{ox} du_{oy} \exp(-u_{ox}^2 - u_{oy}^2) \sum_{k=1}^{k_{\max}(u_{ox}, u_{oy})} (-1)^{k+1} \\
&\quad \times \exp[-u_{\text{lim},k}^2(u_{ox}, u_{oy})] \\
&\approx \frac{1}{\pi} \sum_i \sum_j \Delta u_{ox,i} \Delta u_{oy,j} \exp(-u_{ox,i}^2 - u_{oy,j}^2) \sum_{k=1}^{(k_{\max})_{i,j}} (-1)^{k+1} \\
&\quad \times \exp[-(-u_{\text{lim},k}^2)_{i,j}] \tag{2.5}
\end{aligned}$$

which is in a form suitable for numerical summation. The quantities  $u_{\text{lim},1}$ ,  $u_{\text{lim},2}$ ,  $\dots$ ,  $u_{\text{lim},k_{\max}}$  are the values of  $u_{oz}$  for which  $H$  changes between 0 and 1 for each  $u_{ox}$  and  $u_{oy}$ . These values must be found by numerically determining which particle orbits reimpact the surface. These orbits can, however, be determined in analytic form, with time as a parameter. To do this, we use the coordinate system shown in Fig. 3, together with a  $y$ -axis (not shown) directed into the plane of the Figure. The equation of motion for an electron is:

$$\dot{\mathbf{v}} = -\frac{e}{m} (\mathbf{E} + \mathbf{v} \times \mathbf{B}). \tag{2.6}$$

We solve this with the initial conditions  $\xi = y = \eta = 0$ ,  $v_{\xi} = v_{o\xi}$ ,  $v_y = v_{oy}$ , and  $v_{\eta} = v_{o\eta}$ . We introduce the dimensionless variables:

$$\begin{aligned}
\epsilon_x &= \frac{E_x}{B} \sqrt{\frac{\pi m}{2kT}}, \quad \epsilon_y = \frac{E_y}{B} \sqrt{\frac{\pi m}{2kT}}, \quad \text{etc;} \\
\tilde{x} &= x/\bar{a}, \quad \tilde{y} = y/\bar{a}, \quad \text{etc;} \tag{2.7}
\end{aligned}$$

$$\tau = \omega_c t = (eB/m)t.$$

In the present discussion,  $\epsilon_x$  and  $\epsilon_y$  are both zero, but for later use (Secs. 4 and 5), we have retained these quantities in the formulas below. We obtain:

$$u_{o\xi} = u_{ox} \sin \theta + u_{oz} \cos \theta;$$

$$u_{o\eta} = -u_{ox} \cos \theta + u_{oz} \sin \theta;$$

$$\tilde{\xi} = \frac{-1}{\pi} \epsilon_\xi \tau^2 + \frac{2}{\sqrt{\pi}} u_{o\xi} \tau;$$

(2.8)

$$\tilde{y} = \left\{ \frac{2}{\sqrt{\pi}} u_{oy} - \frac{2}{\pi} \epsilon_\eta \right\} \sin \tau + \left\{ \frac{2}{\sqrt{\pi}} u_{o\xi} + \frac{2}{\pi} \epsilon_y \right\} (\cos \tau - 1) + \frac{2}{\pi} \epsilon_\eta \tau;$$

$$\tilde{\eta} = \left\{ \frac{2}{\sqrt{\pi}} u_{o\eta} + \frac{2}{\pi} \epsilon_y \right\} \sin \tau + \left\{ \frac{2}{\sqrt{\pi}} u_{oy} - \frac{2}{\pi} \epsilon_\eta \right\} (1 - \cos \tau) - \frac{2}{\pi} \epsilon_y \tau;$$

$$\tilde{z} = \tilde{\xi} \cos \theta + \tilde{\eta} \sin \theta.$$

Equations (2.8) can also be differentiated to find  $d\tilde{z}/d\tau$ . The numerical procedure for finding the quantities  $u_{lim,k}$  in Eq. (2.5) then involves calculating  $\tilde{z}$  and  $d\tilde{z}/d\tau$  at a succession of points along an orbit (the electron will reimpact during the first gyroperiod  $0 < \tau \leq 2\pi$  if at all, so this interval always suffices), and making the appropriate tests on these quantities to find out whether the orbit reimpacts or escapes. For each  $u_{ox,i}$  and  $u_{oy,j}$ , this is done for a succession of values of  $u_{oz}$ . These tests also yield the local minimum of  $\tilde{z}(\tau)$  if one exists. Whenever a change occurs between no escape and escape from one such value of  $u_{oz}$  to the next, an interpolation using these minima can be used to provide the corresponding value of  $u_{lim,k}$ . In cases where they are unavailable, the arithmetic mean of the two successive  $u_{oz}$

values is used.

We have chosen the abscissas  $u_{ox,i}$  and  $u_{oy,j}$  in Eq. (2.5) by first solving numerically the transcendental equation  $\frac{1}{2} + \frac{1}{2} \operatorname{erf}(u_k/\sqrt{2}) = k/n$  for  $k = 1, 2, \dots, n-1$ . The resulting values  $u_k$  then subdivide the normalized Gaussian distribution  $\exp(-u^2)/\sqrt{\pi}$  into  $n$  "slices" whose areas decrease as  $\exp(-\frac{1}{2}u_k^2)$  when  $n$  is large. In terms of these  $u_k$ , we then choose values  $u_{o,k}$  at the centroids of these slices, and weights  $c_k$  equal to the areas under each. We obtain:

$$u_{o,k} = \frac{\exp(-u_k^2) - \exp(-u_{k-1}^2)}{\sqrt{\pi}(\operatorname{erf} u_k - \operatorname{erf} u_{k-1})} \quad (2.9)$$

$$c_k = \frac{1}{2}(\operatorname{erf} u_k - \operatorname{erf} u_{k-1}) \quad (2.10)$$

for  $k = 1, 2, \dots, n$ . A convenient method for calculating the required values of  $\operatorname{erf} u = 1 - \operatorname{erfc} u$  has been given by Shepherd and Laframboise (1981). The resulting values  $u_{o,k}$  are then used to provide the required values of  $u_{ox,i}$  and  $u_{oy,j}$ , and the  $c_k$  are used to provide values of  $(1/\sqrt{\pi}) \Delta u_{ox,i} \exp(-u_{ox,i}^2)$  and  $(1/\sqrt{\pi}) \Delta u_{oy,j} \exp(-u_{oy,j}^2)$ , for use in Eq. (2.5). We have provided values of  $u_{oz}$  for use in determining the  $u_{lim,k}$  values in Eq. (2.5) by solving the equation  $1 - \exp(-u_{oz,k}^2/2) = k/n$  for  $k = 0, 1, 2, \dots, n-1$ . This gives  $u_{oz,k} = \{2 \ln[1/(1-k/n)]\}^{1/2}$ ; these values are distributed most densely near  $u_{oz} = 0$ , but still densely enough at large  $u_{oz}$  that the resulting intervals give vanishing flux contributions in this limit. This completes the definition of the procedure used for calculating the ratio  $I/I_o$  of escaping to emitted flux.

### 3. RESULTS AND DISCUSSION FOR $\mathbf{E}$ NORMAL TO SURFACE

Escaping secondary-electron current densities, computed as described in Sec. 2, are shown in Table I and Fig. 5. Each value of  $i = I/I_0$  was calculated using  $80 \times 80 \times 40$  orbits, whose initial velocity components  $u_{ox}$ ,  $u_{oy}$ , and  $u_{oz}$  were chosen as described in Sec. 2, and with points on the orbits calculated at intervals  $\Delta\tau = \pi/45$ . For 8 values of  $\epsilon$  and 11 values of  $\theta$ , the resulting calculation took about 100 hr total on a Hewlett-Packard 1000F minicomputer with Vector Instruction Set. The results are accurate to within about 0.2% or better. The result for  $\epsilon = 0$  is just the analytic result  $i = \cos \theta$ . To see why this is so, we consider the electron orbit shown in Fig. 6, which has been fictitiously extended so as to pass through the surface and re-emerge from it. In the absence of an electric field ( $\epsilon = 0$ ), this orbit has the same speed at the re-emergence point C as at the emission point A. Since we have also assumed that the emitted velocity distribution is isotropic, and therefore a function of speed only, the real orbit, for which C is the emission point, must carry the same population as would the fictitious re-emerged orbit. The flux crossing the reference surface DE, which is  $\perp \mathbf{B}$ , is therefore the same as if such passages and re-emergences actually occurred, and is the same as if another reference surface FG, also  $\perp \mathbf{B}$ , were emitting electrons having the same velocity distribution. However, in reality, the electrons come from the real surface HJ, which is not  $\perp \mathbf{B}$ , and all the electron-orbit guiding centers which are inside any given magnetic-flux tube through DE will also be inside the

projection of the same flux tube onto HJ, and the ratio of the intersection areas of this tube with HJ and DE is just  $\sec \theta$ . The ratio of escaping to emitted flux must therefore be the reciprocal of this, or  $\cos \theta$ , as stated above.

Also evident in Fig. 5 is the fact, mentioned in Sec. 2, that when  $\epsilon$  is large enough, electron escape becomes essentially complete except when  $\theta$  is very nearly  $90^\circ$ . This means that in Shuttle high-voltage charging conditions, for which  $30 \leq \epsilon \leq 120$  (Sec. 2), the occurrence of high-voltage charging in marginal circumstances may depend very strongly on the precise orientation of a surface. A slowly-rotating surface which passes through tangentiality to **B** may experience a sudden, brief high-voltage charging event. For the same reason, attempts to predict high-voltage charging may be afflicted by "sensitivity" problems: if one attempts to predict "worst-case" charging by assuming that secondary electrons do not escape, then the resulting predictions are likely to be overly pessimistic most of the time. On the other hand, if one assumes that secondaries do escape, correct predictions will be obtained almost all of the time, but occasionally a large underestimate of charging will occur.

In a real situation, **E** would not be uniform, but would decrease with distance from the surface, contrary to our assumptions. Our results can therefore be expected to overestimate electron escape. This would probably not be a large effect, but this presumption remains to be verified. An approximate compensation for it can be made by calculating  $\epsilon$  using an electric field value which is averaged over the first mean gyroradius distance from the surface.

The results in Table 1 are approximated to within 2.5% of  $I_0$  by the empirical formula:

$$\begin{aligned}
 a &= 1 + 1.35\epsilon^{1.1394} \exp \left\{ 0.083725 \left\{ 1 + \tanh \left[ 1.9732 \ln \left( \frac{\epsilon}{1.13} \right) \right] \right\} \right. \\
 &\quad \left. - 0.07825 \ln \left[ 1 + (\epsilon/8.5)^{1.78148} \right] \right\}; \\
 b &= 0.38033c^{0.95892} \exp \left\{ 2.0988 \left\{ 1 + \tanh \left[ 1.49 \ln \left( \frac{\epsilon}{3.26} \right) \right] \right\} \right\}; \\
 c &= \ln (90^\circ/\theta); \\
 i &= \cos [90^\circ \exp(-ac-bc^2)].
 \end{aligned} \tag{3.1}$$

This formula also has the correct limiting behavior when  $\epsilon \rightarrow 0$  or  $\infty$ , or  $\theta \rightarrow 0^\circ$  or  $90^\circ$ . An approximation formula for the emitted flux is also available [Eqs. (5) and (6) of Laframboise et al (1982a), and Laframboise and Kamitsuma (1983)]. The results presented in this Section have already been presented by Laframboise (1985).

#### 4. THEORY FOR NON-NORMAL DIRECTIONS OF E

If a spacecraft surface is charged to a nonuniform potential, the electric field  $E$  outside it has a nonzero component tangential to the surface. The resulting problem geometry is more complicated, and two additional angles,  $\alpha$  and  $\psi$ , which define the direction of the electric force  $-eE$ , need to be specified (Fig. 7).

It may then happen that even though  $-eE$  is still directed away from the

surface, its projection along the direction of  $\mathbf{B}$  is directed toward the surface, as shown in Fig. 8a. This happens when the angle between  $-e\mathbf{E}$  and either  $\mathbf{B}$  or  $-\mathbf{B}$ , whichever is outward, is greater than  $90^\circ$ . The resulting situation is analogous to that for a sailboat tacking against the wind (Fig. 8b): even though the resultant wind force on the sail has a downwind component, its projection parallel to the boat's direction of motion (roughly along its centreline) has an upwind component, and the boat therefore moves upwind.

When this situation exists, every emitted electron returns to the surface, and the escaping flux is zero. The resulting situation then differs from that shown in Fig. 5 in at least one important respect. The range of surface orientations (relative to  $\mathbf{B}$ ) for which electron escape is entirely prevented, is no longer infinitesimal (at  $\theta = 90^\circ$ ), but finite, and this may greatly enlarge the portion of a spacecraft's surface for which secondary-electron escape is not available as a discharge mechanism.

Even though no electrons escape under these conditions, the possibility exists that they may travel a relatively long distance, equal to many gyro-radii, parallel to the surface before returning. This may produce relatively large surface currents, and these may modify substantially the charge distribution on the spacecraft. The question of surface currents resulting from migration of reimpacting electrons along the surface is to be examined in a subsequent paper (J.G. Laframboise, to be published). Here, we point out only one general feature of this charge migration. The general motion of an emitted

electron is a superposition of gyromotion about  $\mathbf{B}$ , an  $\mathbf{E} \times \mathbf{B}$  drift, and an acceleration in the  $-\mathbf{eE}$  direction. The  $\mathbf{E} \times \mathbf{B}$  drift direction may have either an inward or outward normal component. If it is outward, migration distances over the surface will be larger, and so therefore will surface currents. Since  $\mathbf{B}$  is in the  $(x,z)$  plane, the  $z$ -component of  $\mathbf{E} \times \mathbf{B}/B^2$  is  $-B_x E_y/B^2$ . For  $B_x > 0$ , this component has a sign opposite to that of  $E_y$ . Therefore, when  $E_y < 0$  [region (3) in Fig. 9], the migration distance of reimpacting electrons, and therefore also the surface currents produced by them, are likely to be much larger than when  $E_y > 0$  [region (2) in Fig. 9]. These surface currents will be primarily along the tangential projection of the  $\mathbf{E} \times \mathbf{B}$  drift direction, rather than of  $-\mathbf{eE}$ , so they may have little effect on helping to discharge the spacecraft.

These predictions are based on the assumption that  $\mathbf{E}$  and  $\mathbf{B}$  are spatially uniform. However, if average migration distances become equal to many gyroradii, it is then more likely that this assumption will be seriously in error, and many of our predictions, especially the quantitative ones presented in Sec. 5, may then become unreliable.

Before we present computed results, we need to determine, in terms of the angles  $\theta$ ,  $\alpha$ , and  $\psi$  in Fig. 7, when the projection of  $-\mathbf{eE}$  along  $\mathbf{B}$  is directed toward the surface. This projection is:

$$(-e\mathbf{E} \cdot \mathbf{B})\mathbf{B}/B^2 \quad (4.1)$$

The z-component of this is:

$$\begin{aligned} & -e(E_x B_x + E_z B_z) B_z/B^2 \\ & = -eE \cos^2 \theta \cos \alpha (1 + \tan \alpha \cos \psi \tan \theta) \end{aligned} \quad (4.2)$$

Since  $-eE \cos^2 \theta \cos \alpha > 0$ , this means that escape is prevented if:

$$\tan \alpha \cos \psi \tan \theta < -1, \quad (4.3)$$

or equivalently:

$$\begin{aligned} \theta & < \tan^{-1} (-\cot \alpha \sec \psi), \text{ for } 0 \leq \psi < 90^\circ; \\ \theta & > \tan^{-1} (-\cot \alpha \sec \psi), \text{ for } 90^\circ < \psi \leq 180^\circ. \end{aligned} \quad (4.4)$$

## 5. RESULTS AND DISCUSSION FOR NON-NORMAL DIRECTIONS OF E.

Figures 10 - 17 show escaping secondary-electron current densities  $i \equiv i(\alpha, \psi, \theta, \epsilon)$  when  $-e\mathbf{E}$  is not normal to the spacecraft surface ( $\alpha \neq 0^\circ$ ). Details of the computations of these results are the same as those given in Secs. 2 and 3, except that  $64 \times 64 \times 32$  orbits were used for calculating each value of  $i$ , and the results are accurate to about 0.4% or better.

In Figs. 10 and 11,  $\psi = 0^\circ$ , so  $-e\mathbf{E}$ ,  $\mathbf{B}$ , and the surface normal are coplanar. The  $\mathbf{E} \times \mathbf{B}$  drift direction is therefore tangential to the surface. In Fig. 10, no electrons escape ( $i = 0$ ) when  $-90^\circ \leq \theta < -60^\circ$  because the acceleration of

all electrons along  $\mathbf{B}$  is toward the surface, as discussed in Sec. 4. For  $\theta > -60^\circ$ , this acceleration is away from the surface, but it is larger for  $\theta > 0^\circ$  than for  $\theta < 0^\circ$ , so increasing the electric field magnitude  $\epsilon$  increases electron escape more for  $\theta > 0^\circ$ . For  $\theta > -60^\circ$ ,  $i = \cos \theta$  when  $\epsilon = 0$ , as was the case for  $-e\mathbf{E}$  normal to the surface (Fig. 5). Some care is needed in defining what is meant by the case " $\epsilon = 0$ ". For  $-90^\circ \leq \theta < -60^\circ$ ,  $i = 0$  in the limit  $\epsilon \rightarrow 0+$ , but in the limit  $\epsilon \rightarrow 0-$ , the electric field is reversed, so  $i = \cos \theta$  in this limit, and  $i$  therefore has a discontinuity at  $\epsilon = 0$ . The discontinuity is reversed for  $\theta > -60^\circ$ . However, we are interested here primarily in cases when  $\epsilon > 0$  (negatively-charged spacecraft surfaces), so in this work, we take " $\epsilon = 0$ " to mean the limiting case  $\epsilon \rightarrow 0+$ . In Fig. 11,  $\alpha$  has been increased from  $30^\circ$  to  $60^\circ$ , so the effects just discussed in connection with Fig. 10 are seen again, but more strongly. This time, escape is suppressed completely for  $-90^\circ \leq \theta < -30^\circ$ .

In Fig. 12, the acceleration of electrons along  $\mathbf{B}$  is toward the surface, and therefore  $i = 0$ , for  $\theta < \tan^{-1}(-\sqrt{6}) = -67.79^\circ$ , as given by Eq. (4.4). Also, we now have  $\psi \neq 0^\circ$ , so the electric force vector is no longer in the same plane as  $\mathbf{B}$  and the surface normal. As a result, the  $\mathbf{E} \times \mathbf{B}$  drift now has a nonzero normal component. This decreases electron escape for  $\theta < 0^\circ$ , and increases it for  $\theta > 0^\circ$ . It also causes the escape to remain nonzero at  $\theta = 90^\circ$ . As before, the larger outward acceleration along  $\mathbf{B}$  also increases escape for  $\theta > 0^\circ$ . For  $\theta$  just larger than  $67.79^\circ$ , we see that escape is suppressed almost completely for larger values of  $\epsilon$ ; this is because the inward direction of the  $\mathbf{E} \times \mathbf{B}$  normal component causes most electrons to reimpact the surface

during the first gyroperiod after emission. In Fig. 13,  $\alpha$  has been increased from  $30^\circ$  to  $60^\circ$ , with consequent enhancement of the effects just discussed. We now have  $i=0$  for  $\theta < \tan^{-1}(-\sqrt{2/3}) = -39.23^\circ$ .

In Figs. 14 and 15,  $\psi = 90^\circ$ , and the projection of  $-eE$  along  $\mathbf{B}$  is away from the surface for all  $\theta$ , so suppression of electron escape by deceleration along  $\mathbf{B}$  does not occur. However, for  $\theta$  close to  $-90^\circ$ , the effect of the inward direction of the  $\mathbf{E} \times \mathbf{B}$  normal component overcomes the effect of the outward acceleration along  $\mathbf{B}$ , especially because  $\mathbf{B}$  is now nearly tangential to the surface, and therefore electron escape is effectively suppressed for larger values of  $\epsilon$ . In Fig. 15, suppression for  $\epsilon = 20$  is essentially complete over a range of  $\theta$  values extending more than  $30^\circ$  on either side of  $\theta = -90^\circ$ .

In Figs. 16 and 17, we have  $\psi = 135^\circ$ , and the effects of electron deceleration along  $\mathbf{B}$  and of  $\mathbf{E} \times \mathbf{B}$  drift now suppress electron escape at opposite ends of the range of  $\theta$ . From Eq. (4.4), we now have  $i = 0$  for  $\theta > \tan^{-1}(\sqrt{6}) = 67.79^\circ$  and  $\theta > \tan^{-1}(\sqrt{2/3}) = 39.23^\circ$ , respectively. In Fig. 16, the  $\mathbf{E} \times \mathbf{B}$  effect significantly enhances electron escape as  $\theta$  increases, just before the deceleration effect cuts it off.

The results shown in Fig. 5 and Figs. 10-17 encompass, albeit rather sparsely, the entire range of possible directions of  $\mathbf{B}$  and  $\mathbf{E}$  for  $\alpha$  up to  $60^\circ$ . To see this, we first note that in the important case where  $-eE$  is normal

to the surface, the  $i$  values for  $-90^\circ \leq \theta \leq 0^\circ$  can be generated from those for the range  $0^\circ \leq \theta \leq 90^\circ$ , which is covered in Fig. 5; this can be seen by rotating the  $\mathbf{B}$  vector in Fig. 7 by  $180^\circ$  about the  $z$  axis. Secondly, the  $i$  values for  $\alpha = 30^\circ$  and  $60^\circ$  and  $\psi = 180^\circ, 225^\circ, 270^\circ,$  and  $315^\circ$  can be generated from those in Figs. 10-17 by rotating the  $\mathbf{B}$  and  $-e\mathbf{E}$  vectors in Fig. 7 together about the  $z$  axis by  $180^\circ$ . The effect of this is to increase all the  $\psi$  values by  $180^\circ$  and also to reverse the sign of  $\theta$ . Finally, we can obtain the  $i$  values for cases where  $\mathbf{B}$  is reversed by first noting that reversal of  $\mathbf{B}$  implies reversal of both the  $\xi$  coordinate in Fig. 7 (in order that  $\xi$  remain parallel to  $\mathbf{B}$ ) and the  $\eta$  coordinate [in order that the  $(\xi, y, \eta)$  axes remain right-handed]. The quantities  $\sin \theta, \cos \theta, u_{o\xi}, u_{o\eta}, \tilde{\xi}, \epsilon_\xi,$  and  $\epsilon_\eta$  in Eq. (2.8) will then all reverse. To keep  $z \equiv z(\tau)$  in Eq. (2.8) unchanged, we require also that  $\tilde{\eta}$  reverse, and we therefore require that  $\epsilon_y$  and  $u_{oy}$  also be reversed. However, the emitted velocity distribution is symmetric in  $u_{oy}$ , and reversing  $\epsilon_y$  involves replacing the angle  $\psi$  by  $360^\circ - \psi$ , and this replacement gives back the same set of  $\psi$  values for which our computations already give  $i$ .

We can summarize the results in Figs. 10-17 by noting that when  $\alpha \neq 0$ , two new mechanisms, which were not present when  $-e\mathbf{E}$  was normal to the surface (Fig. 5), can suppress electron escape. These are: an inward normal component of  $\mathbf{E} \times \mathbf{B}$ , if  $\epsilon$  is strong enough, and a decelerating projection of  $-e\mathbf{E}$  along  $\mathbf{B}$ , for any  $\epsilon > 0$ . These may act at the same end or at opposite ends of the range of magnetic-field directions  $-90^\circ \leq \theta \leq 90^\circ$ . These mechanisms can greatly enlarge the range of surface orientations for which escape is suppressed.

## 6. CALCULATION OF SECONDARY-ELECTRON DENSITIES

Once the secondary-electron escape fluxes are known (Secs. 3-5), a simple, inexpensive, approximate calculation of their space-charge density distribution can be set up. The proposed method is as follows: (1) ignore the gyromotion of the secondary electrons once they have escaped. Their motion then involves: (a) an acceleration along magnetic field lines, of amount  $-(e/m)\mathbf{E}\cdot\mathbf{B}/B$  (b) a drift motion of velocity  $\mathbf{E} \times \mathbf{B}/B^2$  across magnetic field lines. (2) Integrate enough of the trajectories defined by this motion (i.e. their guiding-center trajectories) to define trajectory tubes whose cross-section at any point can be calculated with sufficient accuracy; the method described by Laframboise et al (1982b, Sec. 7), can be used to calculate the area of a trajectory tube without reference to neighbouring trajectories. (3) Calculate their space-charge density  $n(\mathbf{r})$  at any point by (a) ignoring the "thermal" spread of their velocities (b) then invoking the fact that their density  $\times$  their velocity [as given by the orbit integration mentioned in (2)],  $\times$  the cross-sectional area  $A(\mathbf{r})$  of the trajectory tube (which must be calculated in a plane  $\perp$  the trajectory) at the point  $\mathbf{r}$  in question, = a constant (whose value is given by the initial conditions at the point on the spacecraft where the trajectory originates) (c) finding their velocity at the point in question by using energy conservation, together with the values of electric potential  $\phi(\mathbf{r})$  and  $\phi_0$  at that point and the emission point, and their assumed velocity  $v_0$  at the emission point. The result is:

$$n(\mathbf{r}) = n_0 v_0 A_0 / \left\{ A(\mathbf{r}) \sqrt{v_0^2 + (2e/m) [\phi(\mathbf{r}) - \phi_0]} \right\} \quad (6.1)$$

where  $n_0 v_0$  is the escaping flux calculated in Secs. 3-5. At most positions,  $n(r)$  will be insensitive to the precise value assumed for  $v_0^2$ ; assuming that  $v_0 = \text{the one-sided thermal speed } (2kT/\pi m)^{1/2}$  will suffice for most purposes.

### ACKNOWLEDGMENTS

This work was supported by the U.S. Air Force Geophysics Laboratory under Contract No. F19628-83-K-0028.

### REFERENCES

- Al'pert, Ya.L., Gurevich, A.V., and Pitaevskii, L.P., *Space Physics with Artificial Satellites*, Consultants Bureau, New York, 1965.
- Katz, I., and Parks, D.E., Space shuttle orbiter charging. *J. Spacecraft and Rockets* 20, 22-25, 1983.
- Laframboise, J.G., Calculation of secondary-electron escape currents from inclined spacecraft surfaces in a magnetic field. In: *Spacecraft Environmental Interactions Technology 1983*, edited by C.K. Purvis and C.P. Pike, NASA Conference Publication 2359/Report No. AFGL-TR-85-0018, Air Force Geophysics Laboratory, Massachusetts, pp. 277-286, 1985.

- Laframboise, J.G., Kamitsuma, M., The threshold temperature effect in high-voltage spacecraft charging. In: Proc. Air Force Geophys. Lab. Workshop on Natural Charging of Large Space Structures in Near Earth Polar Orbit, edited by R.C. Sagalyn, D.E. Donatelli, and I. Michael, Report No. AFGL-TR-83-0046/Environmental Research Paper No. 825, Air Force Geophysics Laboratory, Massachusetts, pp. 293-308, 1983. ADA134894
- Laframboise, J.G., Kamitsuma, M., and Godard, R., Multiple floating potentials, "threshold-temperature" effects, and "barrier" effects in high-voltage charging of exposed surfaces on spacecraft. In: Proc. Internat. Symp. on Spacecraft Materials in Space Environment, June 1982, Toulouse, France, European Space Agency, Paris, Publication No. ESA SP-178, pp. 269-275, 1982a.
- Laframboise, J.G., Kamitsuma, M., Prokopenko, S.M.L., Chang, Jen-Shih, and Godard, R., Numerical simulation of spacecraft charging phenomena at high altitude, Final Report on Grant AFOSR-76-2962, York University, 1982b.
- Parks, D.E., and Katz, I., Charging of a large object in low polar Earth orbit. In: Spacecraft Charging Technology 1980, NASA Conference Publication 2182/Report No. AFGL-TR-81-0270, Air Force Geophysics Laboratory, Massachusetts, pp. 979-989, 1981. ADA114426
- Shepherd, M.M., and Laframboise, J.G., Chebyshev approximation of  $(1+2x) \exp(x^2) \operatorname{erfc} x$  in  $0 \leq x < \infty$ . Math. of Computation 36, 249-253, 1981.

THETA	EPS	0.00	.20	.50	1.00	2.00	5.00	10.00	20.00
0.00		1.000	1.000	1.000	1.000	1.000	1.000	1.000	1.000
15.00		.964	.990	.999	1.000	1.000	1.000	1.000	1.000
30.00		.865	.930	.977	.997	1.000	1.000	1.000	1.000
45.00		.706	.796	.892	.970	.999	1.000	1.000	1.000
60.00		.499	.585	.704	.856	.982	1.000	1.000	1.000
75.00		.258	.311	.396	.545	.802	.998	1.000	1.000
80.00		.173	.209	.270	.383	.618	.968	1.000	1.000
85.00		.087	.105	.137	.198	.341	.723	.971	1.000
87.00		.052	.063	.082	.119	.209	.487	.810	.991
89.00		.016	.020	.026	.039	.069	.172	.338	.618
90.00		0.000	0.000	0.000	0.000	0.000	0.000	0.000	0.000

TABLE 1

Values of the ratio  $i = I/I_0$  of escaping to emitted flux, for various values of  $\theta$ , the angle (in degrees) between the surface normal and the magnetic field direction, and  $\epsilon$ , the nondimensional repelling electric field strength. These two quantities appear in the table as THETA and EPS, respectively. These results are accurate to within about 0.2% or better. The electric field is normal to the surface.

## FIGURE CAPTIONS

Figure 1. Effect of surface orientation on escape of emitted electrons. In (a), the spacecraft surface is perpendicular to the magnetic field  $\mathbf{B}$ , and the emitted electrons, which experience an electric force  $-e\mathbf{E}$  directed away from the surface, all escape. In (b), the spacecraft surface is nearly parallel to  $\mathbf{B}$ , and almost all of the emitted electrons return to the surface, even though they still experience an electric force directed away from it. Note that the component of  $\mathbf{E}$  perpendicular to  $\mathbf{B}$  results only in an  $\mathbf{E} \times \mathbf{B}$  drift parallel to the surface.

Figure 2. Spacecraft simultaneously in a collisionless ion flow and a magnetic field  $\mathbf{B}$ .

Figure 3. Coordinate system for calculating electron escape fluxes when  $\mathbf{E}$  is perpendicular to the spacecraft surface. The  $y$ -coordinate (not shown) is directed into the plane of the Figure.

Figure 4. Example of an electron orbit having zero initial velocity. The magnetic field  $\mathbf{B}$  is parallel to the  $(x,z)$  plane, and makes an angle  $\theta = 75^\circ$  with the  $z$  axis.  $\epsilon = 1$ . Three gyroperiods of the orbit ( $0 \leq \tau \leq 6\pi$ ) are shown.

Figure 5. Ratio  $i = I/I_0$  of escaping to emitted secondary-electron flux, as a function of the angle  $\theta$  between the surface normal and the magnetic field direction, for various values of the repelling electric field strength parameter  $\epsilon = (E/B) (\pi m/2kT)^{1/2}$ . The electric field is normal to the surface. The result for  $\epsilon = 0$  is given by  $i = \cos \theta$ . Realistic values of  $\epsilon$  for Shuttle high-voltage charging conditions are in the range  $30 \leq \epsilon \leq 120$  (Sec. 2)!

Figure 6. Electron orbit for  $\epsilon = 0$ , fictitiously extended so as to pass through the surface and re-emerge from it.

Figure 7. Problem geometry when potential also varies along surface.

Figure 8. (a) Typical orbit of emitted electron when the electric force  $-eE$  on it has an outward normal component, but the projection of  $-eE$  along  $B$  has an inward normal component (b) analogous situation involving sailboat tacking into wind.

Figure 9. Dependence of secondary-electron escape and surface currents on electric field direction at surface.

Figure 10. Ratio  $i = I/I_0$  of escaping to emitted secondary-electron flux, as a function of the angle  $\theta$  between the surface normal and the magnetic-field direction, for various values of the electric field strength parameter  $\epsilon = (E/B) (\pi m/2kT)^{1/2}$ . Same as Figure 5, except that the electric force vector  $-eE$  is no longer normal to the surface ( $\alpha$  is nonzero).

Figure 11. Same as figure 10, except that  $-eE$  is tilted further away from the surface normal ( $\alpha = 60^\circ$ ).

Figure 12. Same as Figure 10, except that  $-eE$  is no longer in the same plane as the surface normal and the magnetic field vector ( $\psi$  is nonzero).

Figure 13. Same as Figure 12, except that  $-eE$  is tilted further away from the surface normal.

Figure 14. Same as Figures 10 and 12, except that  $\psi = 90^\circ$ .

Figure 15. Same as Figure 14, except that  $-eE$  is tilted further away from the surface normal.

Figure 16. Same as Figures 10, 12, and 14, except that  $\psi = 135^\circ$ .

Figure 17. Same as Figure 16, except that  $-eE$  is tilted further away from the surface normal.

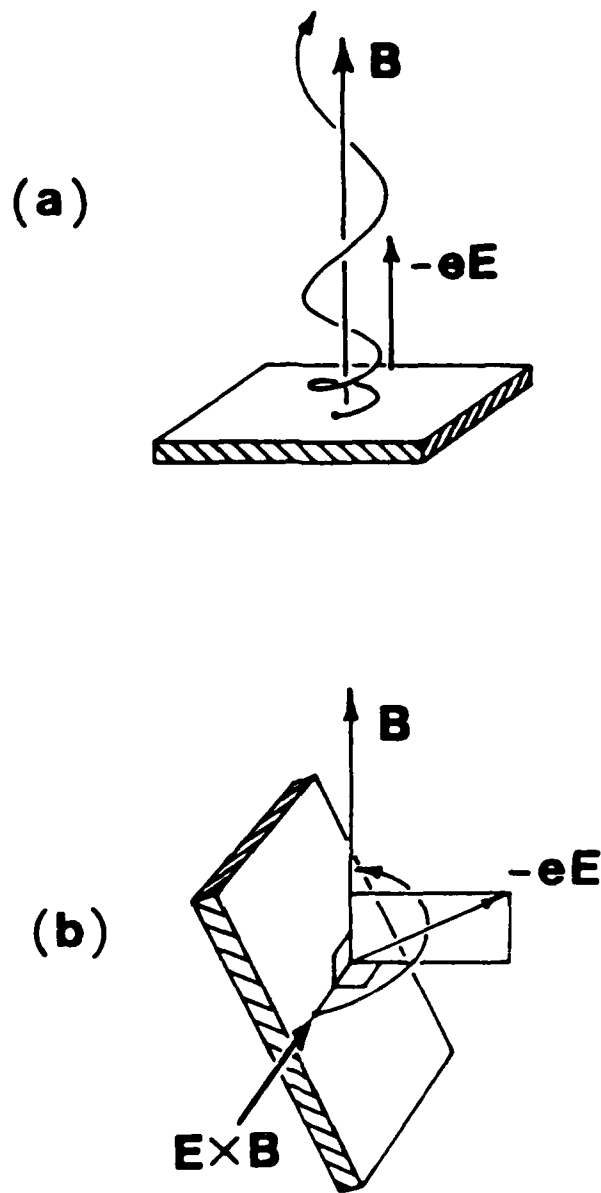


Figure 1. Effect of surface orientation on escape of emitted electrons. In (a), the spacecraft surface is perpendicular to the magnetic field  $\mathbf{B}$ , and the emitted electrons, which experience an electric force  $-\mathbf{eE}$  directed away from the surface, all escape. In (b), the spacecraft surface is nearly parallel to  $\mathbf{B}$ , and almost all of the emitted electrons return to the surface, even though they still experience an electric force directed away from it. Note that the component of  $\mathbf{E}$  perpendicular to  $\mathbf{B}$  results only in an  $\mathbf{E} \times \mathbf{B}$  drift parallel to the surface.

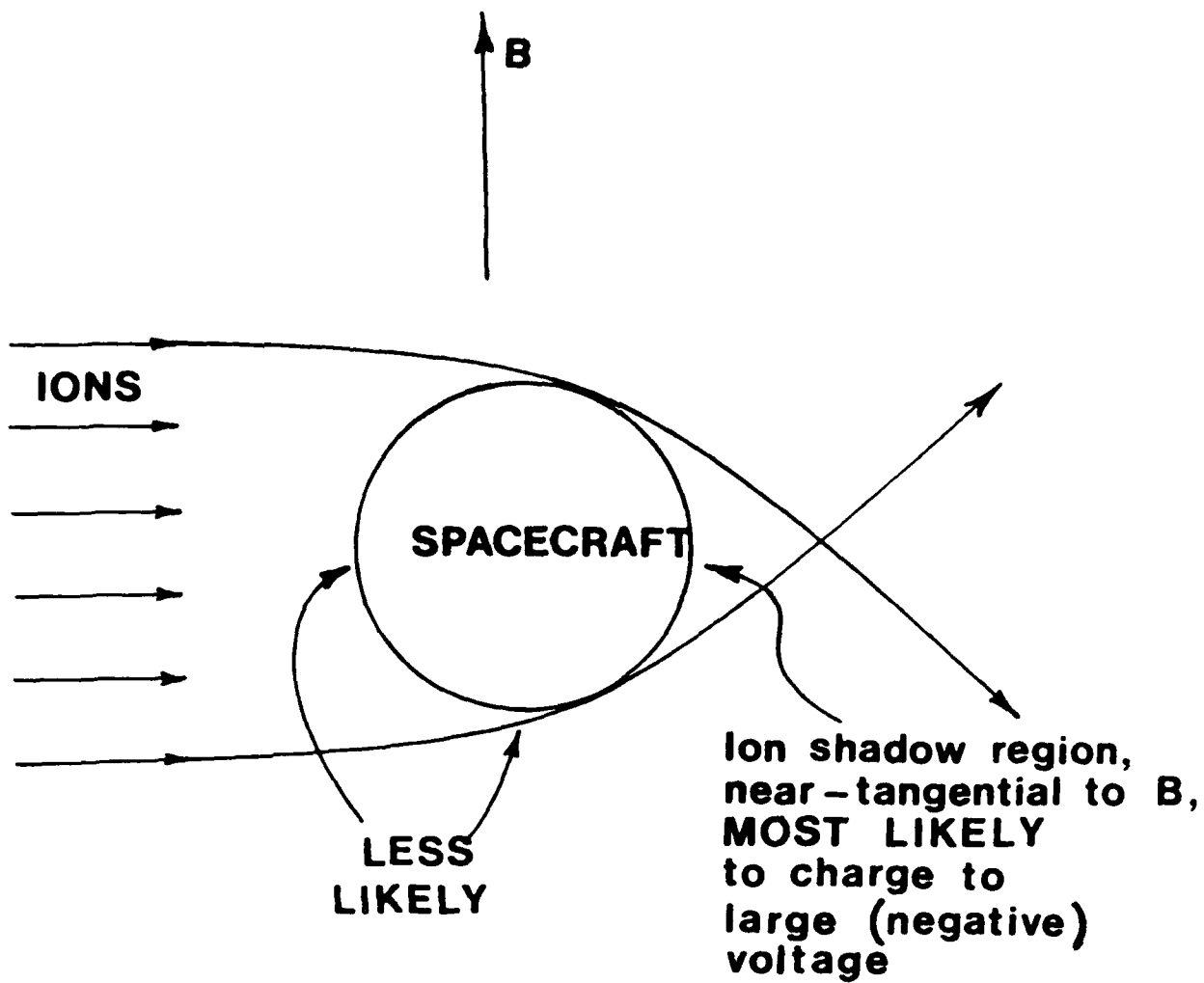


Figure 2. Spacecraft simultaneously in a collisionless ion flow and a magnetic field  $B$ .

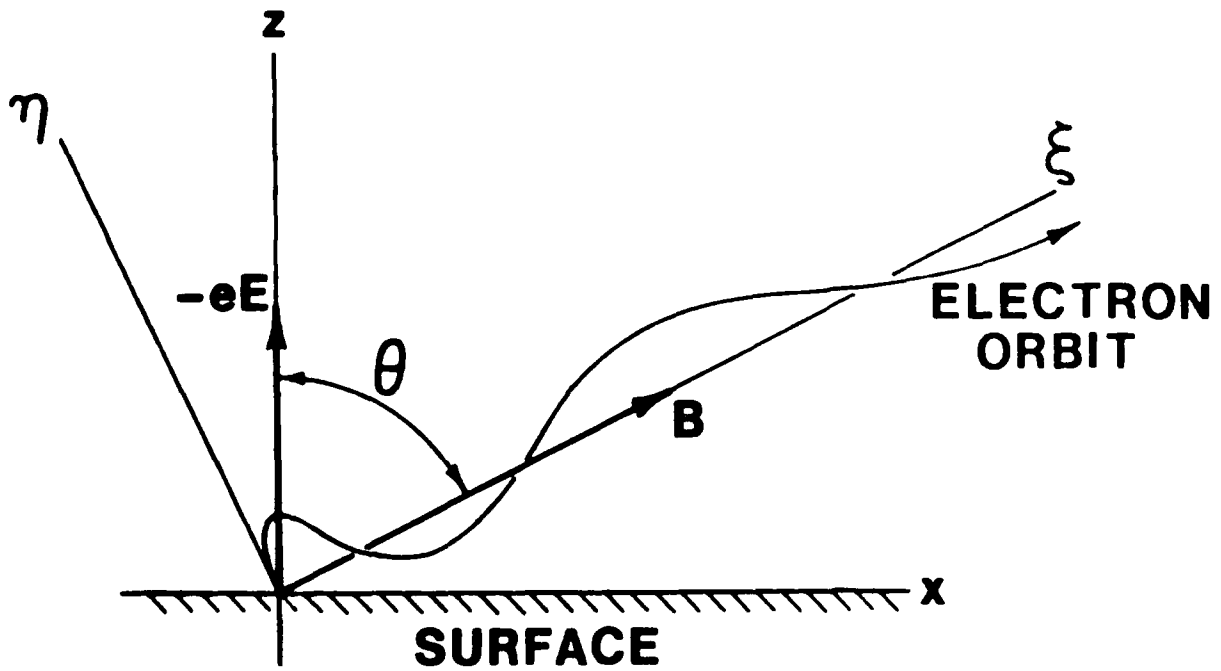


Figure 3. Coordinate system for calculating electron escape fluxes when  $E$  is perpendicular to the spacecraft surface. The  $y$ -coordinate (not shown) is directed into the plane of the Figure.

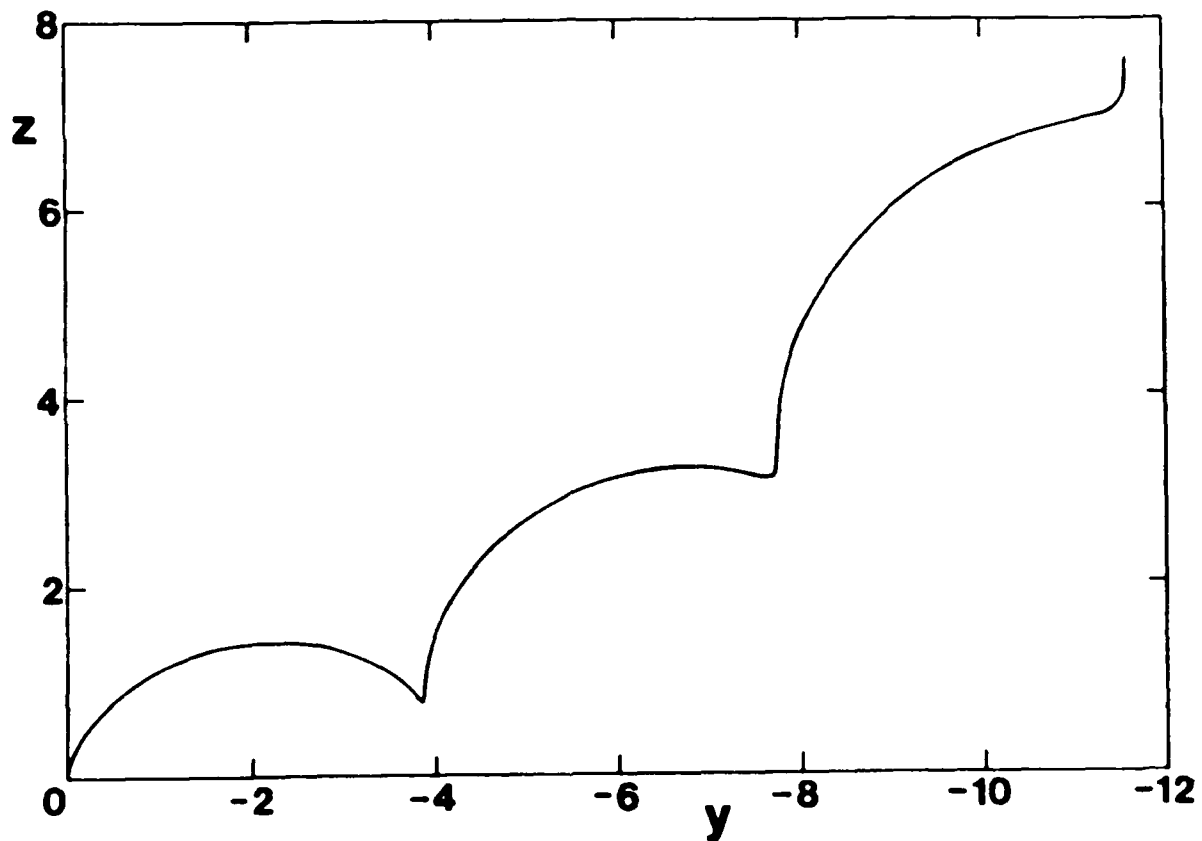


Figure 4. Example of an electron orbit having zero initial velocity. The magnetic field  $\mathbf{B}$  is parallel to the  $(x,z)$  plane, and makes an angle  $\theta = 75^\circ$  with the  $z$  axis.  $\epsilon = 1$ . Three gyroperiods of the orbit ( $0 \leq \tau \leq 6\pi$ ) are shown.

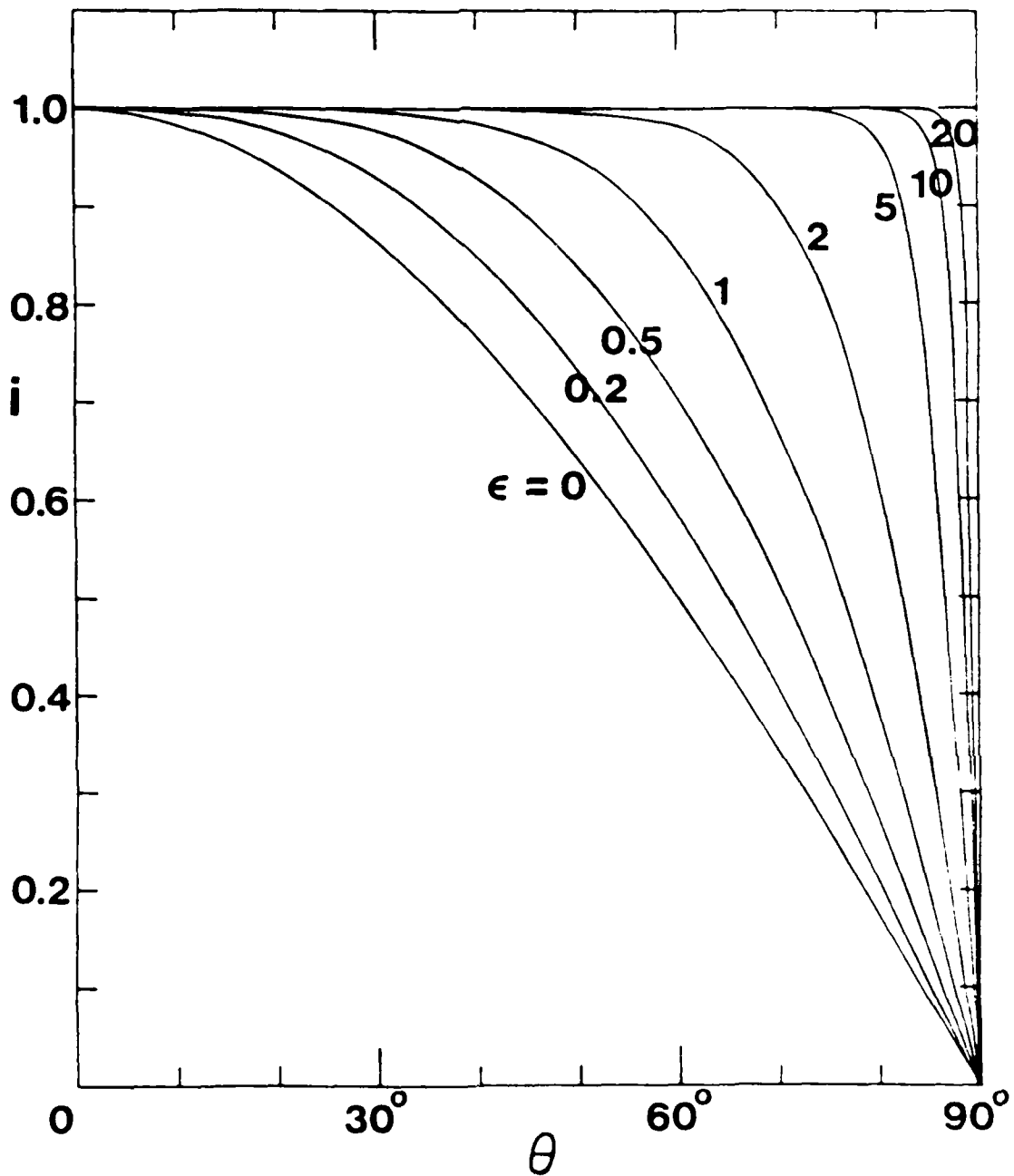


Figure 5. Ratio  $i = I/I_0$  of escaping to emitted secondary-electron flux, as a function of the angle  $\theta$  between the surface normal and the magnetic field direction, for various values of the repelling electric field strength parameter  $\epsilon = (E/B) (\pi m/2kT)^{1/2}$ . The electric field is normal to the surface. The result for  $\epsilon = 0$  is given by  $i = \cos \theta$ . Realistic values of  $\epsilon$  for Shuttle high-voltage charging conditions are in the range  $30 \leq \epsilon \leq 120$  (Sec. 2)!

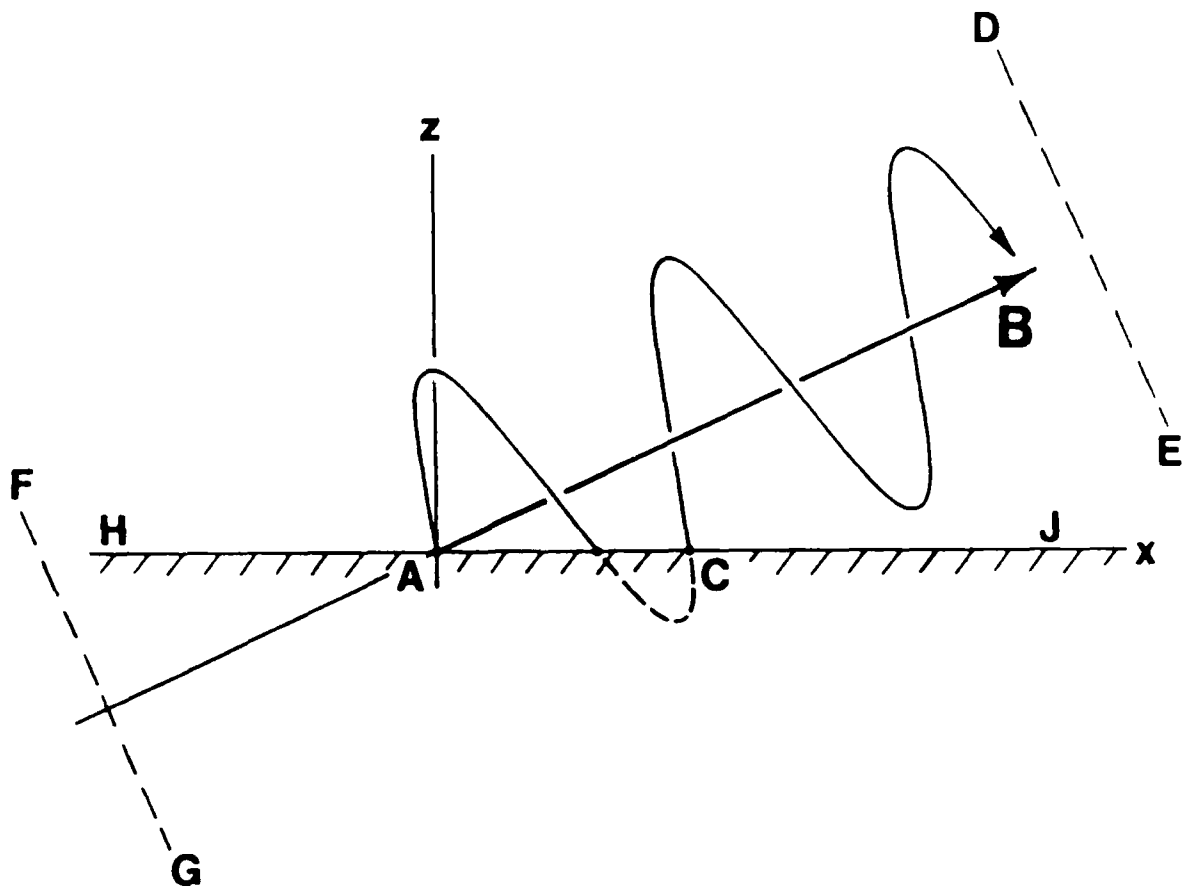


Figure 6. Electron orbit for  $\epsilon = 0$ , fictitiously extended so as to pass through the surface and re-emerge from it.



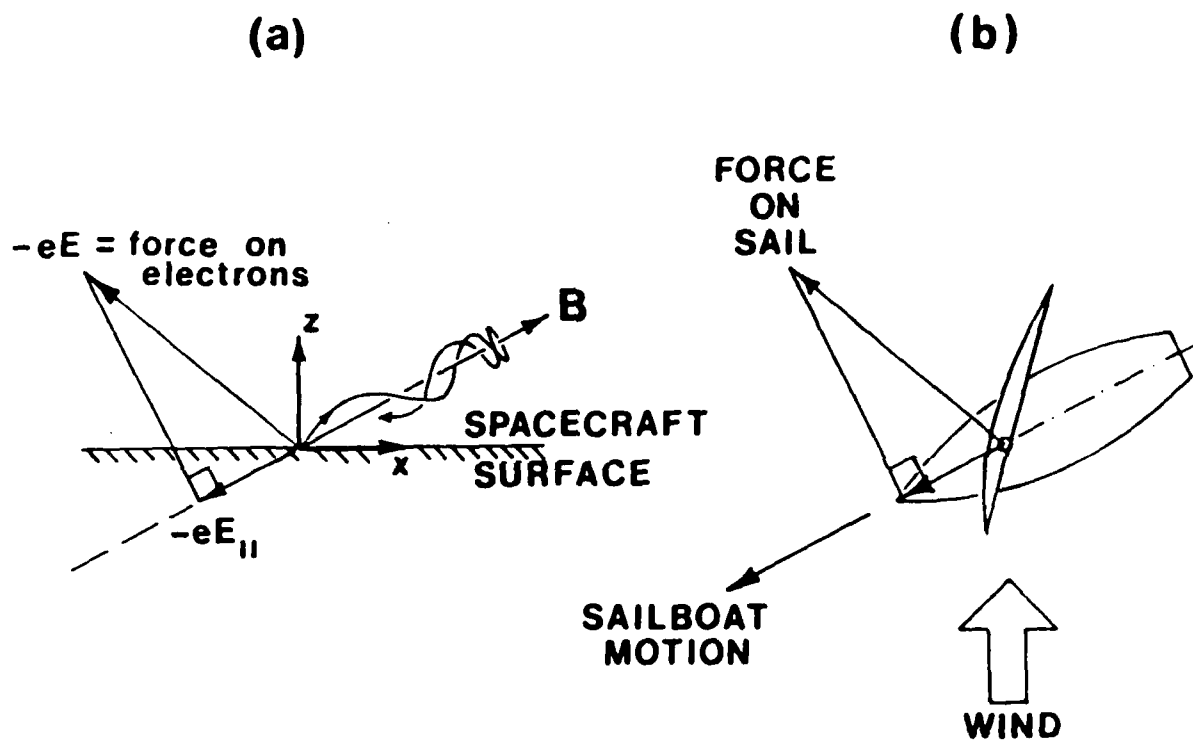


Figure 8. (a) Typical orbit of emitted electron when the electric force  $-e\mathbf{E}$  on it has an outward normal component, but the projection of  $-e\mathbf{E}$  along  $\mathbf{B}$  has an inward normal component (b) analogous situation involving sailboat tacking into wind.

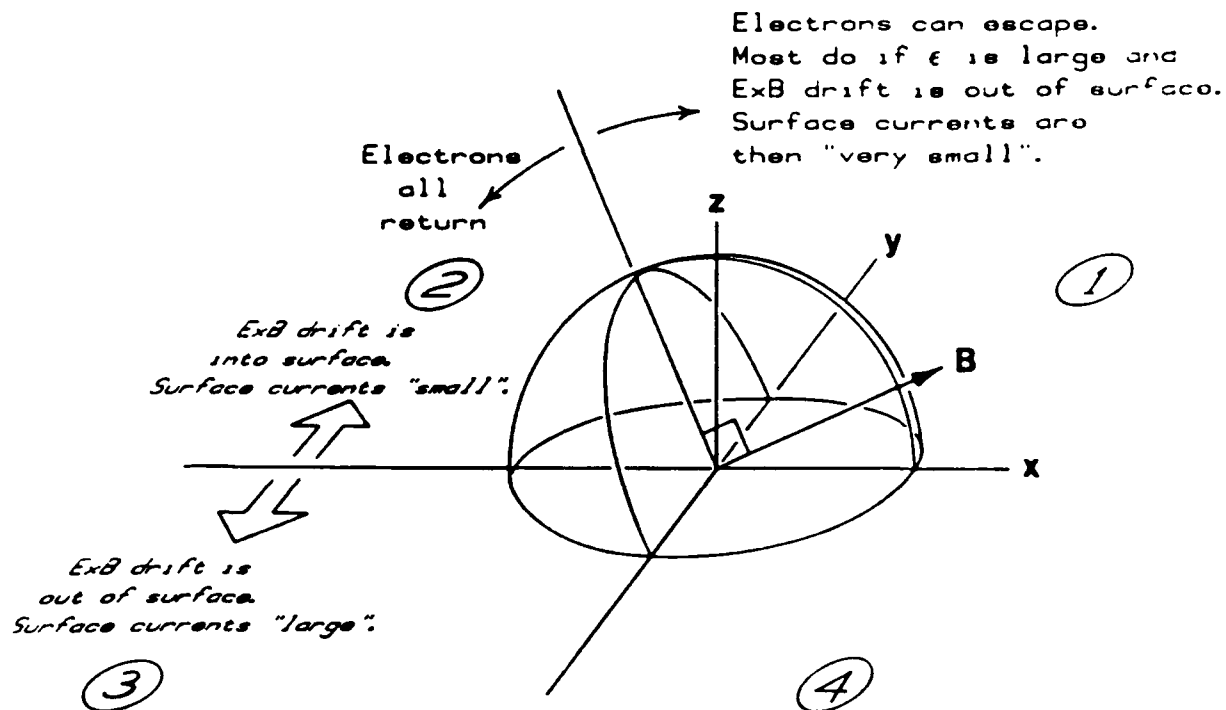


Figure 9. Dependence of secondary-electron escape and surface currents on electric field direction at surface.

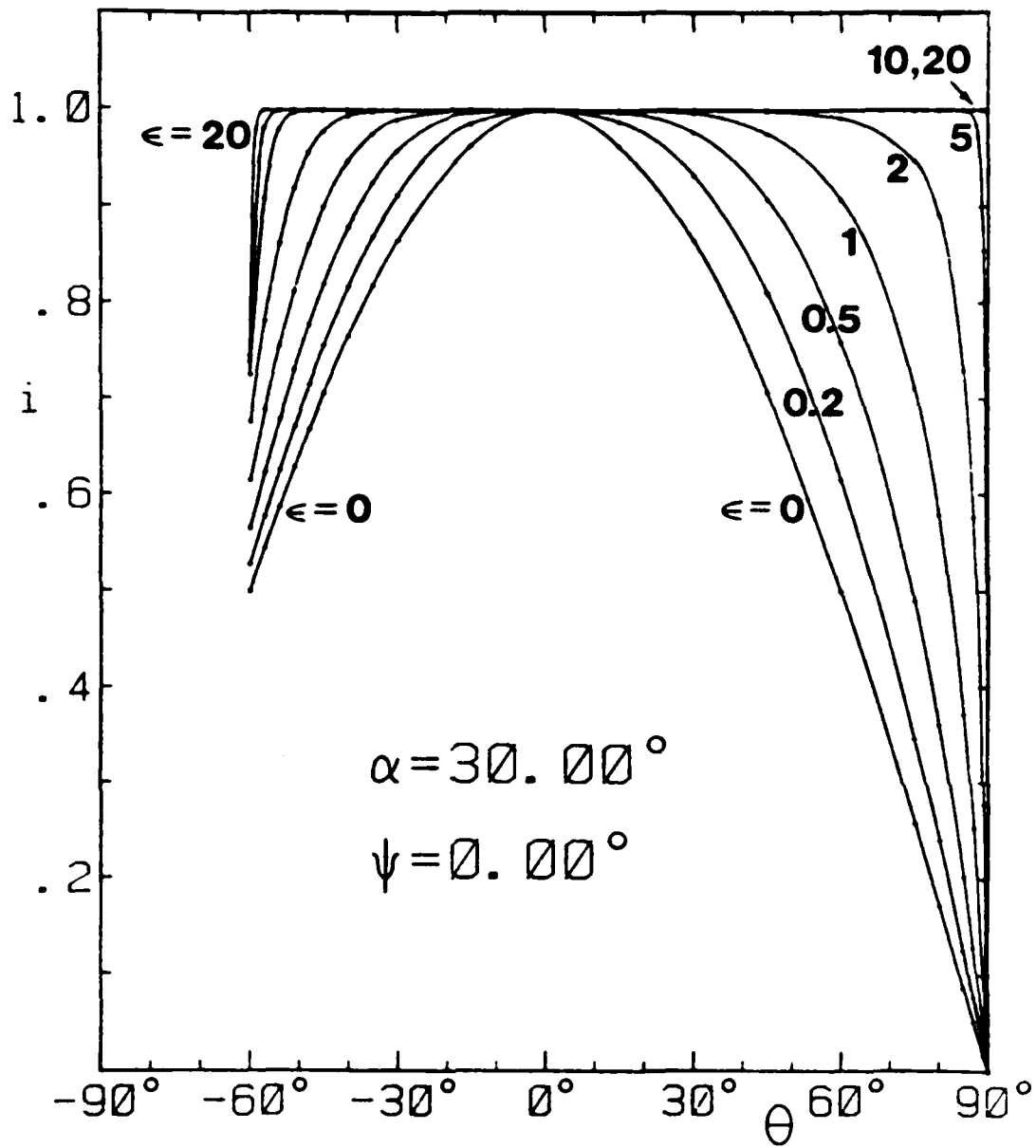


Figure 10. Ratio  $i = I/I_0$  of escaping to emitted secondary-electron flux, as a function of the angle  $\theta$  between the surface normal and the magnetic-field direction, for various values of the electric field strength parameter  $\epsilon = (E/B)(\pi m/2kT)^{1/2}$ . Same as Figure 5, except that the electric force vector  $-eE$  is no longer normal to the surface ( $\alpha$  is nonzero).

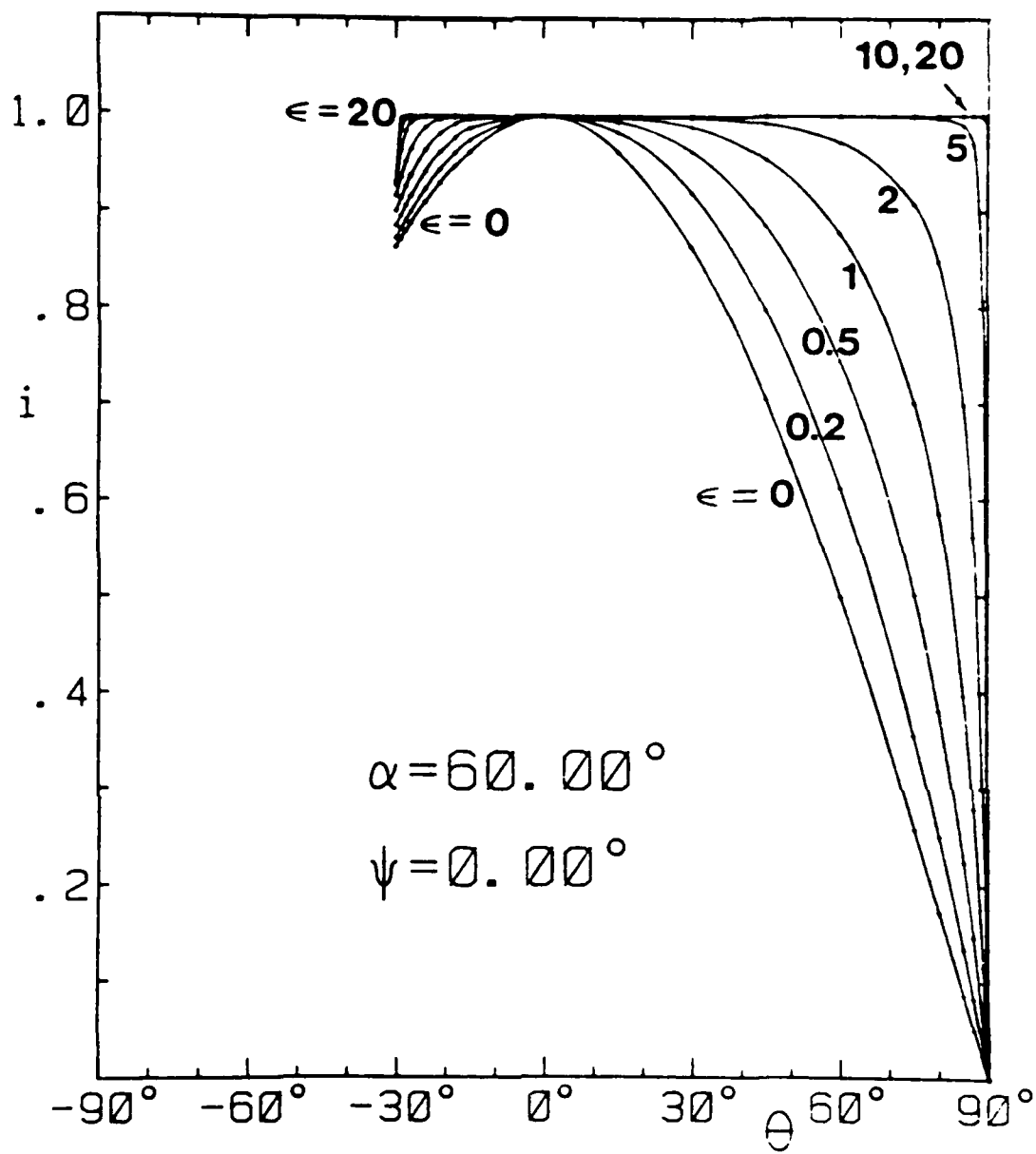


Figure 11. Same as figure 10, except that  $-eE$  is tilted further away from the surface normal ( $\alpha = 60^\circ$ ).

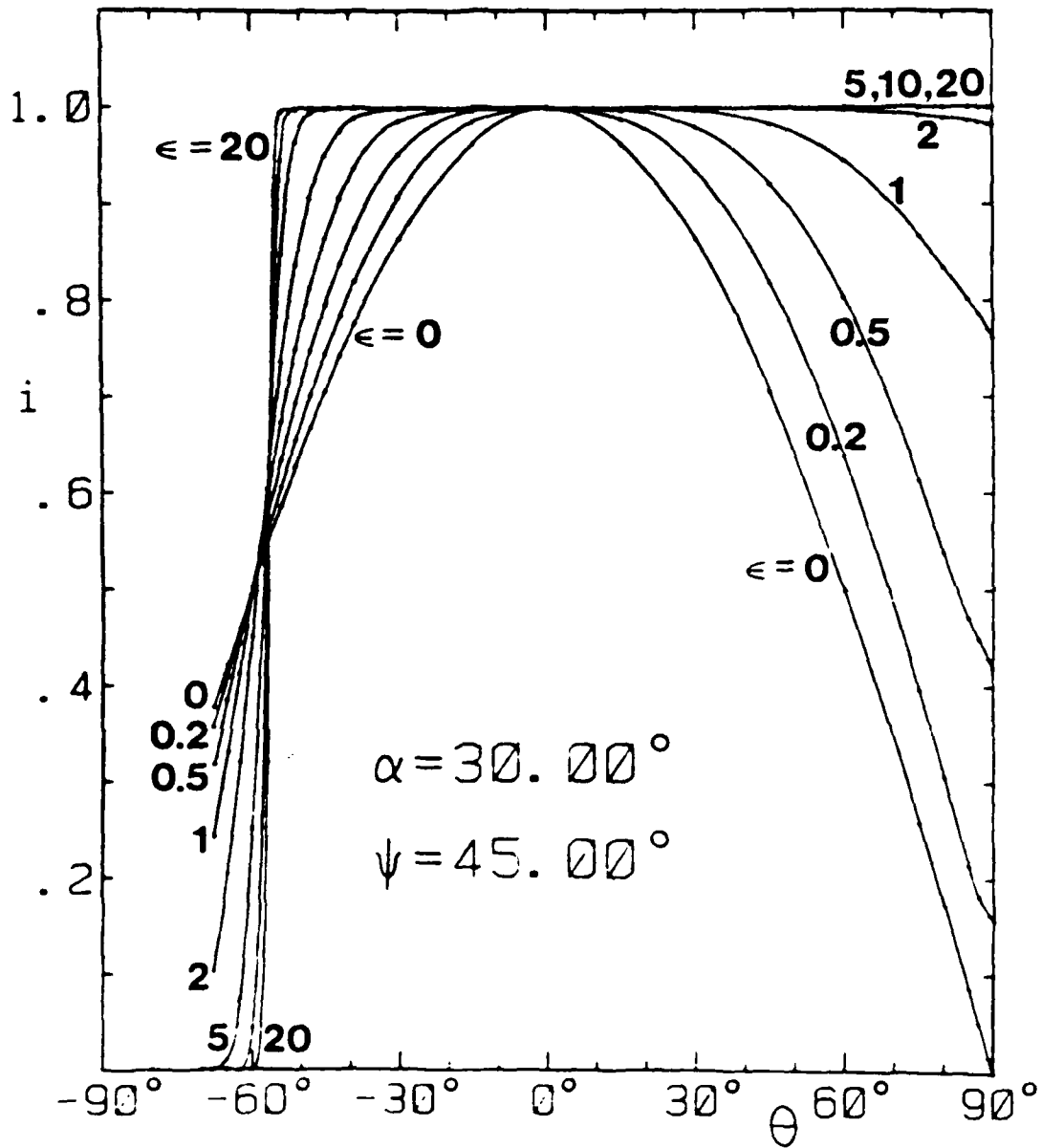


Figure 12. Same as Figure 10, except that  $-eE$  is no longer in the same plane as the surface normal and the magnetic field vector ( $\psi$  is nonzero).

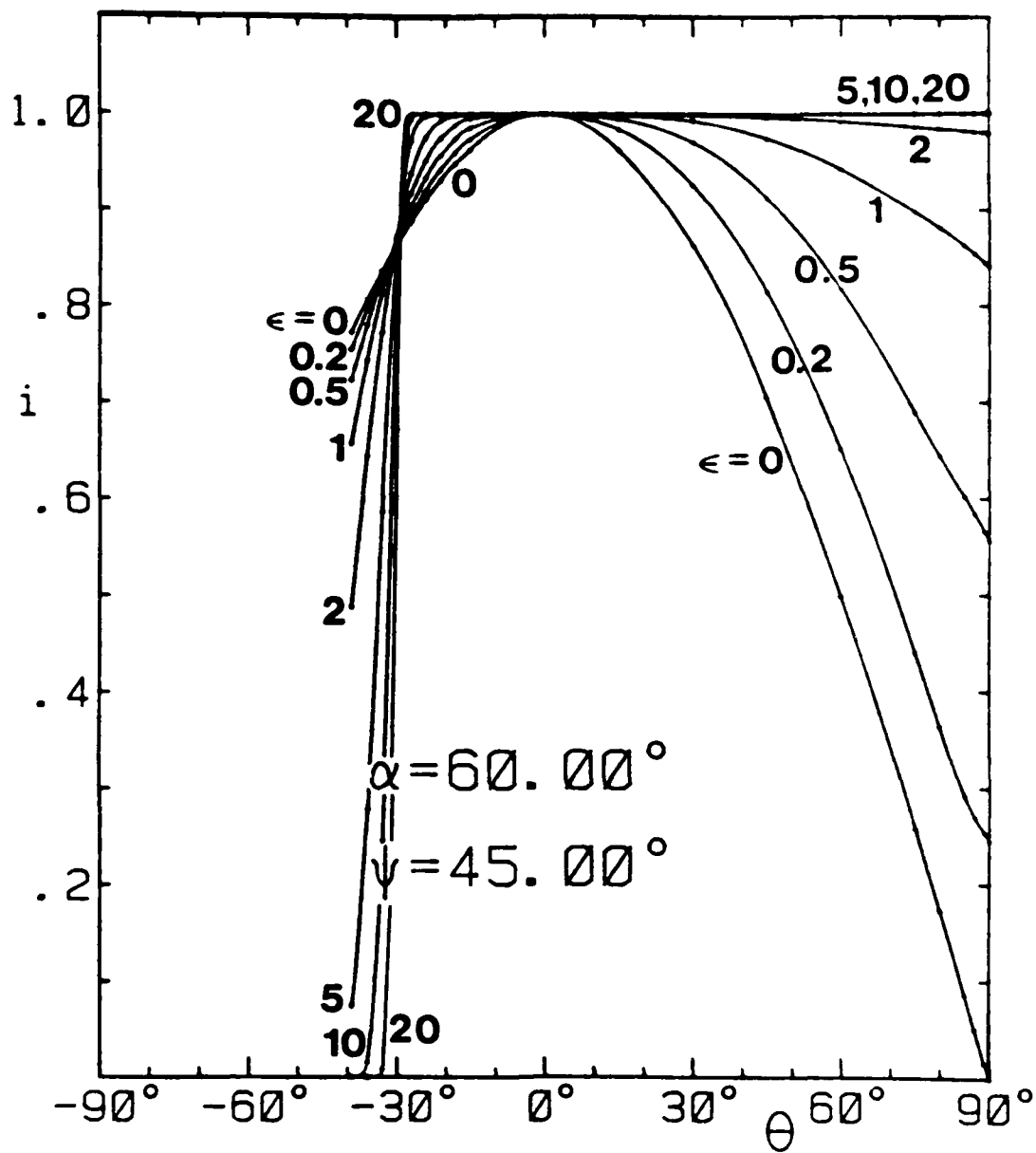


Figure 13. Same as Figure 12, except that  $-eE$  is tilted further away from the surface normal.

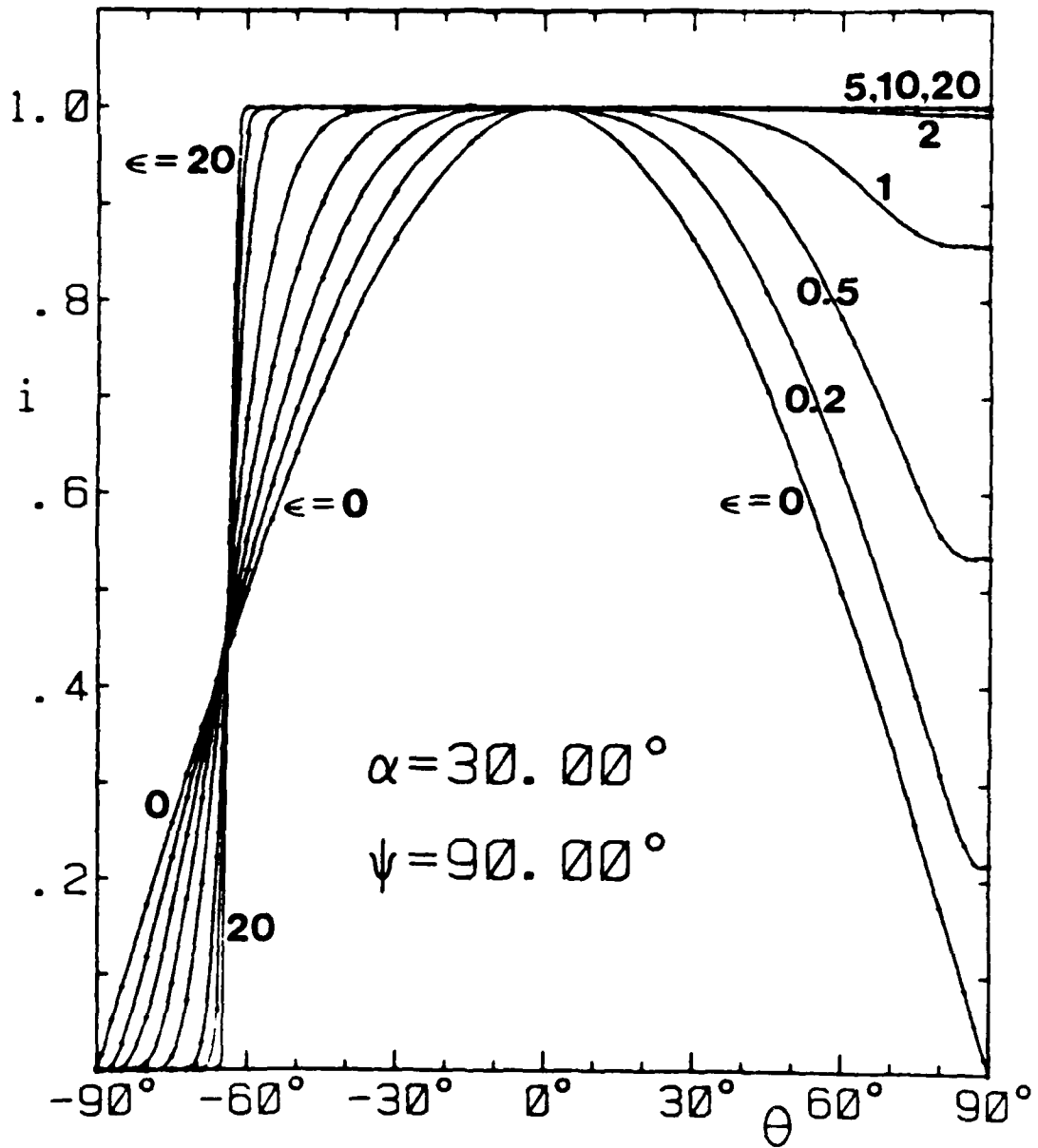


Figure 14. Same as Figures 10 and 12, except that  $\psi = 90^\circ$ .



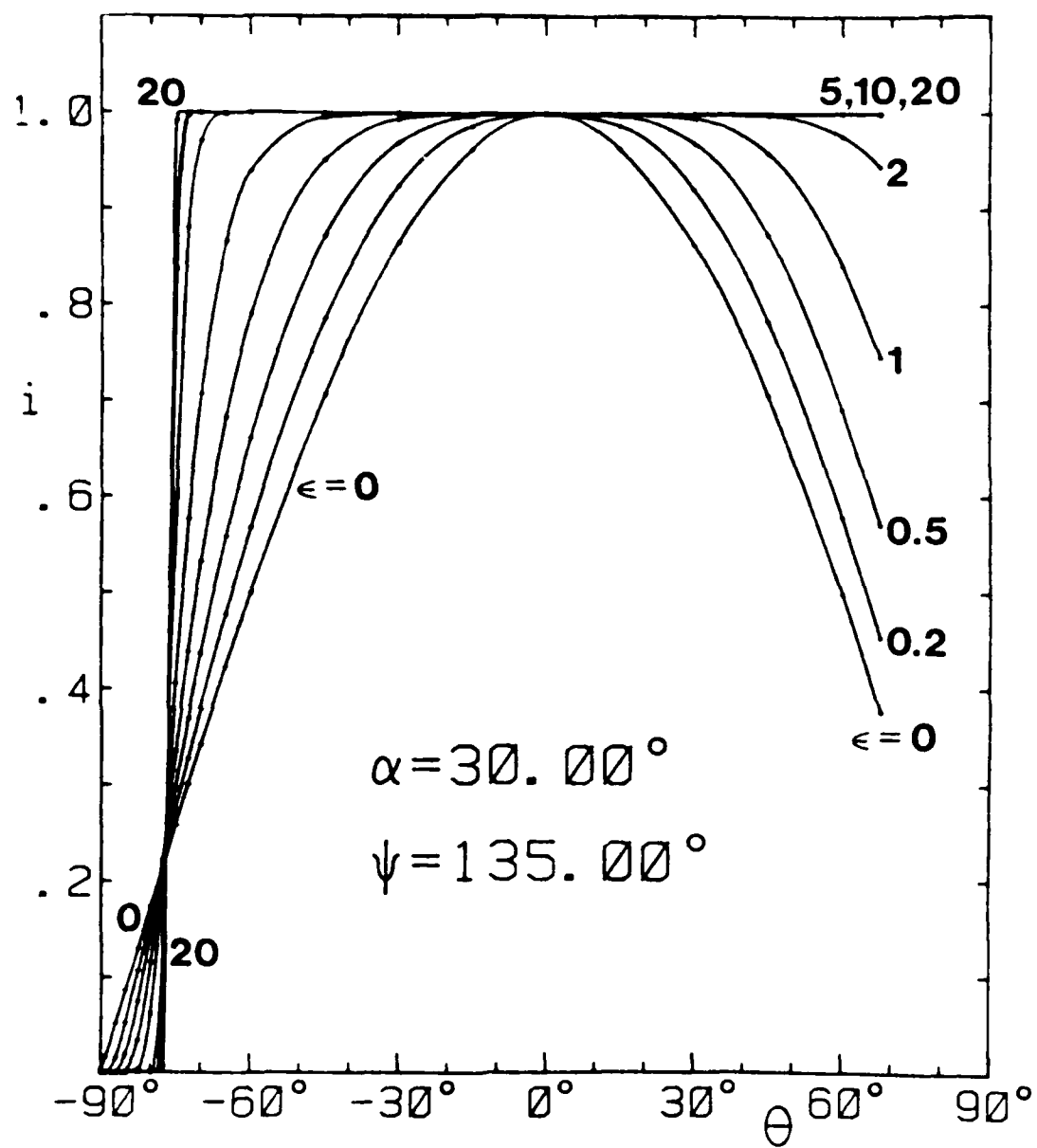


Figure 16. Same as Figures 10,12, and 14, except that  $\psi = 135^\circ$ .

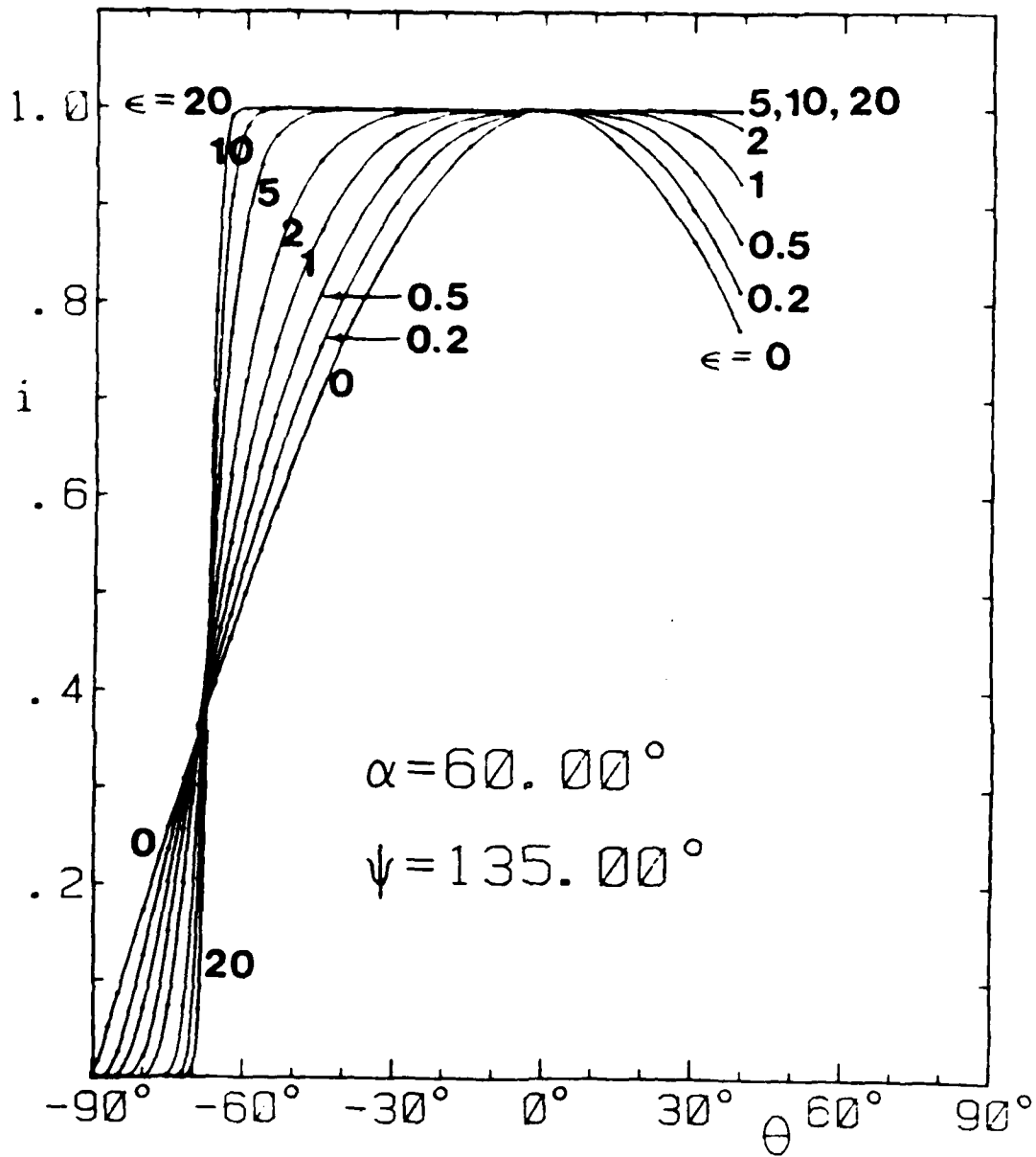


Figure 17. Same as Figure 16, except that  $-eE$  is tilted further away from the surface normal.

END

4-1-87

DTIC